Asian Journal of Chemistry; Vol. 38, No. 7 (2026), 1725-1742
ASIAN JOURNAL OF CHEMISTRY
https://doi.org/10.14233/ajchem.2026.36019

# Structural, Spectroscopic, Thermal, Wavefunction, DFT, Antibacterial and Molecular Docking Investigations on Ethyl 3,4-dihydroxy Benzoate: A Promising Anticancer Agent

S. ASOKAN[1,2], S. SEBASTIAN[1,*], S. SYLVESTRE[3], S. SILVAN[4], R. SAGAYARAJ[1] and S. VANITHA[1]

[1]P.G. & Research Department of Physics, St. Joseph's College of Arts & Science (Autonomous), Cuddalore-607001, India
[2]Department of Physics, Manakula Vinayagar Institute of Technology, Puducherry-605107, India
[3]Department of Chemistry, School of Mathematics and Natural Sciences, Mukuba University, Kitwe 20382, Zambia
[4]P.G & Research Department of Biochemistry, St. Joseph's College of Arts & Science (Autonomous), Cuddalore-607001, India

*Corresponding author: E-mail: sebastian_astro@yahoo.com

*Received*: 16 March 2026 *Accepted*: 16 May 2026 *Published online*: 3 July 2026 AJC-22398

In this study, ethyl 3,4-dihydroxybenzoate (EDB) was investigated through both experimental and density functional theory (DFT) approaches. The optimized molecular geometry was compared with the available single-crystal X-ray diffraction (XRD) data. The FT-IR and FT-Raman spectra were recorded and correlated with the theoretically calculated vibrational wavenumbers, and the potential energy distribution (PED) contributions were analyzed. The UV-Vis absorption spectrum was recorded in the range of 200-800 nm and compared with the results obtained from time-dependent DFT (TD-DFT) calculations. Charge transfer interactions within the molecule were examined using natural bond orbital (NBO) analysis. Thermogravimetric and differential thermal analyses (TG-DTA) were performed to evaluate the thermal stability and decomposition behavior of EDB. Furthermore, frontier molecular orbital (HOMO–LUMO) analysis, electron–hole pair analysis, electron localization function (ELF), localized orbital locator (LOL) and reduced density gradient (RDG) analyses were carried out using the Multiwfn program to gain deeper insight into the electronic structure and intermolecular interactions of the molecule. The antibacterial activity of EDB was evaluated against different bacterial strains, and the minimum inhibitory concentration (MIC) values were determined. In addition, molecular docking studies were performed using AutoDock software to investigate protein–ligand interactions and to assess the potential anticancer activity of EDB against breast and lung cancer targets.

**Keywords: Spectra, Benzoate, Docking, Electron-hole, Reactive descriptor.**

## INTRODUCTION

Aromatic ester compounds derived from benzoic acid have received considerable attention due to their structural diversity and wide spectrum of biological activities. Among them, substituted benzoates have been extensively investigated for their antibacterial, antiviral, antioxidant and anticancer potential [1-4]. The incorporation of electron-donating or electron-withdrawing substituents can significantly modify their physicochemical and pharmacological properties. Therefore, understanding the structural, electronic and biological characteristics of benzoate derivatives is essential for the rational design of new bioactive molecules. The presence of carbonyl group creates protein-ligand interaction boost the anticancer activity by hydrogen bonding formation [5].

Hydrobenzoates have large broad–spectrum antimicrobial properties [6], particularly the 3,4-dihydroxy position, specifically on methyl-2,4-dihydroxybenzoate have remarkable activity. To the best of our knowledge, no comprehensive study integrating experimental characterization, DFT calculations, antibacterial evaluation and molecular docking analysis of ethyl 3,4-dihydroxybenzoate (EDB) has been reported. Therefore, this work combines experimental and theoretical methods to investigate its structural, spectroscopic, electronic, thermal and biological properties. The molecular structure and properties of EDB were investigated using the B3LYP/6-311G-(d,p) level of theory and validated against experimental spectroscopic data. Molecular electrostatic potential (MEP) and HOMO–LUMO analyses were performed to evaluate its electronic characteristics. TG/DTA analysis was conducted to assess thermal behaviour, while RDG and ELF analyses were employed to examine non-covalent interactions and electron density distribution. Furthermore, antibacterial activity and molecular docking studies against breast and lung cancer

targets were carried out to explore the biological potential of ethyl 3,4-dihydroxybenzoate (EDB).

## EXPERIMENTAL

Compound ethyl 3,4-dihydroxybenzoate (EDB), was procured from Sigma-Aldrich Chemicals, Germany, with a purity of 98%. The vibrational spectra were recorded using a Perkin Elmer FT-IR spectrometer in the region 4000–400 $cm^{-1}$ and a Bruker RFS 27 spectrometer in the region 4000-50 $cm^{-1}$ for FT-IR and FT-Raman analyses, respectively. The UV-Visible spectrum was measured from 200 to 600 nm using a UV-1700 series spectrophotometer with ethanol as solvent. The thermal behaviour of EDB was investigated using an SDT Q600 V20 Build 20 thermal analyzer under a nitrogen atmosphere from 30 to 1000 ºC.

**Minimal inhibitory concentration (MIC) assay:** To determine the MIC of given sample, a set of Mueller-Hinton broth tubes (5 tubes) were prepared under sterile conditions for each test organism. About 100 µL of each given sample at different concentrations (10, 25, 50, 75 and 100 µg/mL) was added to each Mueller-Hinton broth tubes. Followed by about 10 µL of test culture suspension (each test bacteria) was added to the broth separately and observed for turbid growth. All the tubes were incubated for 24 h at 37 ºC. The lowest concentration of the sample that completely inhibited visible bacterial growth was recorded as the minimum inhibitory concentration (MIC). A control tube containing sterile distilled water and the bacterial inoculum was maintained under identical conditions to compare the microbial growth with the observed in the test tubes.

### Anticancer activity

The human lung cancer (A549) and breast cancer (MCF-7) cell lines were obtained from the National Centre for Cell Science (NCCS), Pune, India and cultured in Eagle's Minimum Essential Medium supplemented with 10% fetal bovine serum (FBS). The cells were maintained at 37 ºC in a humidified atmosphere containing 5% $CO_2$ and 95% air, with routine subculturing performed weekly and medium replacement twice a week. For cytotoxicity studies, the cells were detached using trypsin-EDTA, counted using a hemocytometer and diluted to a final density of $1 \times 10^5$ cells/mL in medium containing 5% FBS. Aliquots of 100 µL of the cell suspension were seeded into 96-well plates at a density of 10,000 cells per well and incubated for 24 h to allow cell attachment. The test samples were dissolved in DMSO, serially diluted to obtain five different concentrations and 100 µL of each dilution was added to the respective wells containing 100 µL of culture medium. Following treatment, the cells were incubated for an additional 48 h under the same culture conditions [7,8]. The cell viability was then assessed using the MTT assay. Briefly, 15 µL of MTT solution (5 mg/mL in phosphate-buffered saline, PBS) was added to each well and incubated for 4 h at 37 ºC. Viable cells reduced the yellow tetrazolium salt, 3-(4,5-dimethylthiazol-2-yl)-2,5-diphenyltetrazolium bromide (MTT), into insoluble purple formazan crystals through the action of mitochondrial succinate dehydrogenase. The culture medium was carefully removed and the resulting formazan crystals were dissolved in 100 µL of DMSO. Absorbance was measured at 570 nm using a microplate reader, with the amount of formazan formed being directly proportional to the number of viable cells. Wells containing medium without the test sample served as the control and all experiments were performed in triplicate**.** The percentage cell viability was calculated with respect to control as follows:

$$\text{Cell viability (\%)} = \frac{[A]\text{test}}{[A]\text{control}} \times 100$$

The % cell inhibition was determined using the following formula:

$$\text{Cell inhibition (\%)} = 100 - \frac{\text{Abs}_{\text{sample}}}{\text{Abs}_{\text{control}}} \times 100$$

Nonlinear regression graph was plotted between % cell inhibition and Log concentration and $IC_{50}$ was determined.

**Computational details:** The theoretical computations were performed on Gaussian 09W software [9] package with Beckee3-Lee-Yang-Parr model with 6-311G(d,p) method as basis set to determine the stable structure by finding minimum energy level in potential energy surface (PES). The Gauss View 5.0 software [10] was used to visualize the molecular structure. The potential energy distribution (PED) of the vibrational modes was calculated using VEDA 4.0 software [11]. Natural bond orbital (NBO) analysis was performed with the NBO 3.1 program [12] implemented in Gaussian 09W [9]. Electronic transitions were investigated using TD-DFT calculations at the B3LYP/6-311G(d,p) level in both gas and solvent phases and correlated with the UV-Vis spectra [13,14]. HOMO-LUMO energies and density of states (DOS) spectra were generated using GaussSum 3.0 [15]. Furthermore, ELF, LOL and RDG analyses were carried out using Multiwfn [16] and the corresponding plots were visualized with VMD 1.9.1 software [17].

**Molecular docking analysis:** Molecular docking analysis was performed to investigate the binding interactions and affinity of the EDB molecule toward selected cancer-related protein targets. Preliminary activity prediction was carried out using the PASS online server [18], which indicated the potential biological activity of EDB against breast and lung cancer targets. The three-dimensional crystal structures of the selected proteins (PDB IDs: 5TWZ and 5C5S) were retrieved from the RCSB Protein Data Bank. Protein preparation, including the removal of water molecules and co-crystallized ligands, was carried out using PyMOL software [19]. Kollman charges and polar hydrogen atoms were assigned using AutoDock Tools (ADT) [20], while the optimized ligand structure was obtained from Gaussian calculations. Molecular docking simulations were performed using AutoDock 4 [21], employing AutoGrid for grid generation [22,23] and the Lamarckian genetic algorithm as the search method. The resulting protein–ligand interactions were analyzed to evaluate the binding characteristics of EDB with the selected targets.

## RESULTS AND DISCUSSION

**Molecular geometry:** The optimised molecular geometry structure of EDB molecule are shown in Fig. 1. The computed

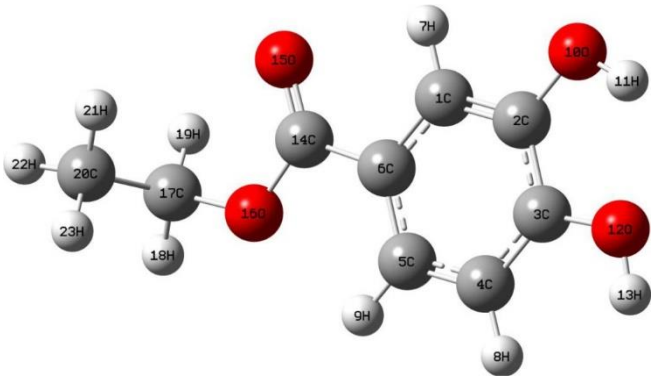


Fig. 1. Optimised molecular structure and atom numbering scheme for ethyl 3,4-dihydroxybenzoate molecule

optimised parameters such as bond length and bond angle are shown in Table-1. There is no crystal data (XRD) available for EDB compound so the related XRD data are shown in Table-1 for comparison of isopropyl 3,4-dihydroxy benzoate [24]. The EDB molecule containing different functional substitutions in the ring system *i.e*. hydroxyl group, ethyl group and oxygen atoms will cause change in the structural and electron properties of EDB molecule. According to the International Tables for Crystallography [25], the typical C=O and C–O bond lengths in carboxylic acid derivatives are approximately 1.266 and 1.351 Å, respectively. In the EDB molecule, the C14=O15 bond length was determined to be 1.215 Å from XRD data [24] and 1.210 Å from B3LYP/6-311G(d,p) calculations, confirming its double-bond character. In contrast, the C14–O16, C2–O10 and C3–O12 bond lengths were calculated as 1.354, 1.361, and 1.372 Å, respectively, which are consistent with single-bond characteristics. The corresponding experimental values also showed good agreement with the theoretical results. These observations indicate that C14=O15 possesses a carbonyl double-bond character, whereas C14–O16, C2–O10 and C3–O12 exhibit predominantly σ-bond character.

The longest bond length in the EDB molecule was observed for the C17–C20 bond, with a calculated value of 1.520 Å at the B3LYP/6-311G(d,p) level. The bond angles C4–C5–C6 and C3–C4–C5 were calculated as 119.73º and 120.00º, respectively, and are in good agreement with the corresponding XRD values of 119.76º and 120.90º [24], indicating that the aromatic ring retains its planarity. The typical C–C bond length in an aromatic ring is approximately 1.40 Å [24,25]. The experimental XRD bond lengths were found to be C1–C2 = 1.376 Å, C2–C3 = 1.391 Å, C3–C4 = 1.380 Å, C4–C5 = 1.381 Å, C5–C6 = 1.389 Å and C1–C6 = 1.386 Å. The corresponding B3LYP/6-311G(d,p) values were 1.385, 1.406, 1.390, 1.392, 1.397 and 1.401 Å, respectively. The close agreement between the theoretical and experimental bond parameters confirms the reliability of the computational model and the delocalized aromatic character of the benzene ring. The slight deviations may be attributed to gas-phase calculations, whereas the XRD data correspond to the condensed crystalline phase of the molecule.

**Mulliken charge analysis:** Mulliken atomic charge analysis was performed at the B3LYP/6-311G(d,p) level to investigate the charge distribution and intramolecular charge-transfer characteristics of the EDB molecule. The calculated atomic charges (Table-2), provide valuable information regarding the electronic environment of individual atoms. All hydrogen atoms possess positive charges ranging from 0.0933 to 0.2665 e, indicating electron deficiency. The carbon atoms C2 and C3 exhibit positive charges of 0.1620 and 0.1339 e, respectively,

TABLE-1
OPTIMISED MOLECULAR STRUCTURE OF EDB MOLECULE
[BOND LENGTH (Å) AND BOND ANGLE (º) BY B3LYP/6-311G(d,p) METHOD

| Parameters | B3LYP/6-311G(d,p) | XRD [24] | Parameters | B3LYP/6-311G(d,p) | XRD [24] | Parameters | B3LYP/6-311G(d,p) | XRD [24] |
|---|---|---|---|---|---|---|---|---|
| Bond length (Å) | | | | | | | | |
| C1-C2 | 1.385 | 1.376 | C4-H8 | 1.086 | 0.930 | O16-C17 | 1.448 | |
| C1-C6 | 1.401 | 1.386 | C5-C6 | 1.397 | 1.389 | C17-H18 | 1.090 | |
| C1-H7 | 1.082 | 0.930 | C5-H9 | 1.081 | 0.930 | C17-H19 | 1.091 | |
| C2-C3 | 1.406 | 1.391 | C6-C14 | 1.488 | 1.479 | C17-C20 | 1.520 | |
| C2-O10 | 1.361 | 1.372 | O10-H11 | 0.966 | 0.820 | C20-H21 | 1.091 | |
| C3-C4 | 1.390 | 1.380 | O12-H13 | 0.962 | 0.820 | C20-H22 | 1.094 | |
| C3-O12 | 1.372 | 1.361 | C14-O15 | 1.210 | 1.215 | C20-H23 | 1.093 | |
| C4-C5 | 1.392 | 1.381 | C14-O16 | 1.354 | 1.330 | | | |
| Bond angle (º) | | | | | | | | |
| C2-C1-C6 | 120.35 | 121.03 | C4-C5-C6 | 119.73 | 119.76 | O16-C17-H18 | 104.21 | |
| C2-C1-H7 | 119.77 | 119.49 | C4-C5-H9 | 120.38 | 120.12 | O16-C17-H19 | 108.72 | |
| C6-C1-H7 | 119.87 | 119.47 | C6-C5-H9 | 119.89 | 120.12 | O16-C17-C20 | 111.48 | |
| C1-C2-C3 | 119.26 | 119.66 | C1-C6-C5 | 120.08 | 119.18 | H18-C17-H19 | 109.53 | |
| C1-C2-O10 | 120.30 | 123.50 | C1-C6-C14 | 117.55 | 117.85 | H18-C17-C20 | 111.50 | |
| C3-C2-O10 | 120.44 | 116.84 | C5-C6-C14 | 122.37 | 122.96 | H19-C17-C20 | 111.14 | |
| C2-C3-C4 | 120.57 | 119.46 | C2-O10-H11 | 107.94 | 109.48 | C17-C20-H21 | 110.62 | |
| C2-C3-O12 | 114.94 | 121.42 | C3-O12-H13 | 110.21 | 109.46 | C17-C20-H22 | 109.79 | |
| C4-C3-O12 | 124.49 | 119.12 | C6-C14-O15 | 124.39 | 123.16 | C17-C20-H23 | 110.81 | |
| C3-C4-C5 | 120.00 | 120.90 | C6-C14-O16 | 112.26 | 113.74 | H21-C20-H22 | 108.27 | |
| C3-C4-H8 | 119.66 | 119.55 | O15-C14-O16 | 123.36 | 123.10 | H21-C20-H23 | 108.99 | |
| C5-C4-H8 | 120.34 | 119.55 | C14-O16-C17 | 116.72 | | H22-C20-H23 | 108.30 | |

TABLE-2
MULLIKEN ATOMIC CHARGE OF EDB MOLECULE CALCULATED BY B3LYP/6-311G(d,p) METHOD

| Atom | Charge | Atom | Charge | Atom | Charge | Atom | Charge |
|---|---|---|---|---|---|---|---|
| C1 | -0.0246 | H7 | 0.1194 | H13 | 0.2665 | H19 | 0.1311 |
| C2 | 0.1624 | H8 | 0.0933 | C14 | 0.4749 | C20 | -0.3095 |
| C3 | 0.1339 | H9 | 0.1031 | O15 | -0.3540 | H21 | 0.1304 |
| C4 | -0.1037 | O10 | -0.3576 | O16 | -0.3530 | H22 | 0.1072 |
| C5 | -0.0227 | H11 | 0.2572 | C17 | -0.0400 | H23 | 0.1123 |
| C6 | -0.2412 | O12 | -0.4020 | H18 | 0.1166 | – | – |

due to the electron-withdrawing influence of the attached hydroxyl oxygen atoms. In contrast, C1, C4, C5, and C6 carry negative charges of -0.0246, -0.1037, -0.0227 and -0.2412 e, respectively. Among all carbon atoms, C14 shows the highest positive charge (0.4749 e), which can be attributed to the presence of two adjacent oxygen atoms (O15 and O16) in the ester group. The oxygen atoms O10, O12, O15 and O16 possess significant negative charges of -0.3576, -0.4020, -0.3540 and -0.3530 e, respectively. Similarly, the methyl carbon atom C20 also carries a negative charge of -0.3095 e (Fig. 2). The observed charge distribution clearly demonstrates electron migration from the carbon framework toward the electronegative oxygen atoms, confirming the existence of intramolecular charge transfer within the EDB molecule.

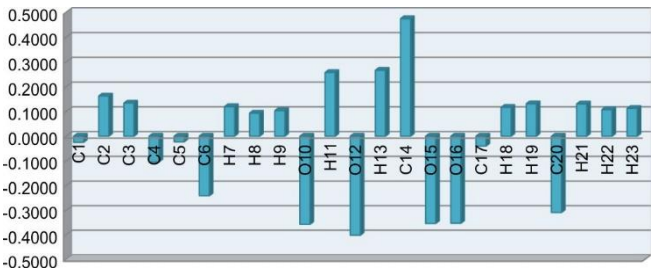


Fig. 2. Mulliken atomic charge for EDB molecule

**Natural bond orbital analysis:** NBO analysis provides insight into the electronic structure and electron density distribution of a molecule in terms of localized Lewis-type orbitals. It is widely used to investigate charge delocalization, donor–acceptor interactions and conjugative effects within molecular systems. The strength of these interactions was evaluated using second-order perturbation theory based on the Fock matrix, where the stabilization energy, $E^{(2)}$, quantifies the interaction between donor (i) and acceptor (j) orbitals [26,27]:

$$E^{(2)} = \Delta E_{ij} = q_i \frac{F(i,j)^2}{E_i - E_j}$$

where $q_i$ denote orbital occupancy, F(i,j) is the off diagonal NBO Fock matrix, $E_i$ and $E_j$ be the diagonal elements.

The interaction between the electron donor and electron acceptor was denoted by $E^{(2)}$ value and are shown in Table-3. A larger $E^{(2)}$ value indicates a stronger donor–acceptor interaction and higher electron delocalization within the molecular system [28]. Normally, the intramolecular interaction formed between C–C, O–H, C–H, C=O, C–O which cause the intermolecular charge transfer (ICT) in the EDB molecule. The electron density (ED) for the conjugate double and single bond lies between ~ 1.62 e to 1.9 e indicate strong delocalisation in the molecule. The most probable interaction happens between C–C bonds, in EDB molecule also C–C bond play a vital role for charge transfer between bonds. The σ(C1-C2) bond distribute bond distribute energy to σ*(C1-C2) of $E^{(2)}$ energy of 4.17 KJ/mol and enhance further to anti bond π*[(C3-C4), (C5-C6)] of $E^{(2)}$ energy 22.19, 19.22 KJ/mol. The same behaviour also found in the bond of σ(C3-C4) to σ*(C2-C3) of 4.62 KJ/mol as $E^{(2)}$ energy values. The bond π(C3-C4) further distribute energy to π*[(C1-C2), (C5-C6)] bond with $E^{(2)}$ value of 17.02 and 20.05 KJ/mol. The similar behaviour are also found to be in C5-C6 bond as shown in Table-3.

Another interaction in the EDB molecule involve electron donating ability of lone pair atoms O10, O12, O15, O16 in σ* and π* bonds. The LP(1)O10→σ*(C2-C3) of 6.46 KJ/ mol and LP(2)O10→σ*(C1-C2) of 27.87 KJ/mol. The LP(1)O12 give σ*(C3-C4) have 6.14 KJ/mol at the same time LP(2)O12 have π*(C3-C4) of energy 25.84 KJ/mol. The similar lone pair LP(1)O15, LP(2)O15, LP(1)O16 and LP(2)O16 are shown in Table-3.

**Vibrational analysis:** The EDB molecule consists of 23 atoms and therefore possesses 63 normal vibrational modes according to the 3N-6 rule. These vibrational modes are distributed into 43 A′ (in-plane) and 20 A″ (out-of-plane) species and the corresponding assignments, IR intensities and Raman activities are shown in Table-4. The potential energy distribution (PED) for each vibrational mode was determined using the VEDA program [11], facilitating reliable spectral assignments. The experimentally recorded FT-IR and FT-Raman spectra, together with the theoretically simulated IR and Raman spectra, are presented in Figs. 3a-b and 4a-b, respectively.

**Ring C–H vibrations:** There are three C–H bond in the ring system as follows: C1-H7, C4-H8 and C5-H9 for the EDB molecule. The aromatic compound shows the presence of C–H vibration between in the range 3100-3000 $cm^{-1}$ [29]. In present study, the three C–H bond recorded in FT-IR spectrum as broad band at 3265 $cm^{-1}$ and 3068 and 3266, 3107, 3080 $cm^{-1}$ in the recorded FT-Raman spectrum corresponds to C–H stretching vibrations as pure mode with PED of ~100%. The computed wavenumber is at 3114, 3104, 3050 $cm^{-1}$ (mode nos. 3-5). The C–H in-plane bending and C–H out-of- plane bending occurs in following region 1300-1000 $cm^{-1}$ and 1000-750 $cm^{-1}$ [30].

In this study, the computed wavenumber at 1300, 1135, 1082 $cm^{-1}$ (mode nos. 22, 29, 31) by B3LYP/6-311G(d,p) method are assigned to C–H in-plane bending vibrations the recorded FT-Raman and FT-IR spectrum are 1295, 1130, 1128 $cm^{-1}$ as a mixed vibrations. The recorded spectrum at 874 $cm^{-1}$

TABLE-3
SECOND ORDER PERTURBATION THEORY ANALYSIS OF FOCK MATRIX IN NBO BASIS FOR EDB BY B3LYP/6-311G(d,p) METHOD

| Donor (i) | Type | ED/e | Acceptor (j) | Type | ED/e | $E^{(2)}$ (Kj/Mol) | E(j)-E(i) (a.u) | F(i,j) (a.u) |
|---|---|---|---|---|---|---|---|---|
| C1-C2 | σ | 1.97320 | C2-C3 | σ* | 0.04126 | 4.17 | 1.23 | 0.064 |
| C1-C2 | π | 1.65629 | C3-C4 | π* | 0.39872 | 22.19 | 0.28 | 0.071 |
| C1-C2 | π | 1.65629 | C5-C6 | π* | 0.39299 | 19.22 | 0.29 | 0.068 |
| C1-C6 | σ | 1.96893 | C2-O10 | σ* | 0.02070 | 3.91 | 1.04 | 0.057 |
| C1-C6 | σ | 1.96893 | C5-C6 | σ* | 0.02322 | 4.65 | 1.26 | 0.068 |
| C1–C6 | σ | 1.96893 | C1-C2 | σ* | 0.02157 | 2.82 | 1.26 | 0.053 |
| C1-H7 | σ | 1.97476 | C2-C3 | σ* | 0.04126 | 4.35 | 1.03 | 0.060 |
| C1-H7 | σ | 1.97476 | C2-O10 | σ* | 0.02070 | 1.12 | 0.86 | 0.028 |
| C1-H7 | σ | 1.97476 | C5-C6 | σ* | 0.02322 | 4.56 | 1.08 | 0.063 |
| C2-C3 | σ | 1.97290 | C1-C2 | σ* | 0.02157 | 4.35 | 1.29 | 0.067 |
| C2-C3 | σ | 1.97290 | C3-C4 | σ* | 0.02597 | 4.42 | 1.27 | 0.067 |
| C2-C3 | σ | 1.97290 | C4-H8 | σ* | 0.01433 | 2.25 | 1.13 | 0.045 |
| C2-O10 | σ | 1.99260 | C3-C4 | σ* | 0.02597 | 1.52 | 1.47 | 0.042 |
| C3-C4 | σ | 1.97730 | C2-C3 | σ* | 0.04126 | 4.62 | 1.25 | 0.068 |
| C3-C4 | π | 1.68864 | C1-C2 | π* | 0.34618 | 17.02 | 0.30 | 0.065 |
| C3-C4 | π | 1.68864 | C5-C6 | π* | 0.39299 | 20.05 | 0.31 | 0.071 |
| C3-O12 | σ | 1.99309 | C1-C2 | σ* | 0.02157 | 1.71 | 1.50 | 0.045 |
| C4-C5 | σ | 1.97307 | C3-O12 | σ* | 0.02356 | 4.65 | 1.02 | 0.062 |
| C4-C5 | σ | 1.97307 | C6-C14 | σ* | 0.06520 | 3.66 | 1.14 | 0.058 |
| C4-H8 | σ | 1.97663 | C2-C3 | σ* | 0.04126 | 4.37 | 1.06 | 0.061 |
| C4-H8 | σ | 1.97663 | C5-C6 | σ* | 0.02322 | 3.74 | 1.11 | 0.057 |
| C5-C6 | σ | 1.97397 | C1-C6 | σ* | 0.02005 | 4.69 | 1.26 | 0.069 |
| C5-C6 | π | 1.66723 | C1-C2 | π* | 0.34618 | 20.47 | 0.28 | 0.068 |
| C5-C6 | π | 1.66723 | C3-C4 | π* | 0.39872 | 18.88 | 0.27 | 0.064 |
| C5-C6 | π | 1.66723 | C14-O15 | π* | 0.26135 | 21.71 | 0.27 | 0.070 |
| C5-H9 | σ | 1.97754 | C1-C6 | σ* | 0.02005 | 4.58 | 1.08 | 0.063 |
| C6-C14 | σ | 1.97003 | C1-C2 | σ* | 0.02157 | 2.63 | 1.23 | 0.051 |
| C6-C14 | σ | 1.97003 | O16-C17 | σ* | 0.03368 | 3.92 | 0.92 | 0.054 |
| O10-H11 | σ | 1.98769 | C1-C2 | σ* | 0.02157 | 4.77 | 1.31 | 0.071 |
| O12-H13 | σ | 1.98885 | C2-C3 | σ* | 0.04126 | 3.81 | 1.29 | 0.063 |
| C14-O15 | π | 1.98409 | C5-C6 | π* | 0.39299 | 4.19 | 0.41 | 0.041 |
| C14-O16 | σ | 1.99189 | C1-C6 | σ* | 0.02005 | 1.61 | 1.48 | 0.044 |
| O16-C17 | σ | 1.98884 | C6-C14 | σ* | 0.06520 | 2.62 | 1.24 | 0.052 |
| C17-H18 | σ | 1.98317 | C14-O16 | σ* | 0.06520 | 3.14 | 0.88 | 0.048 |
| C17-H19 | σ | 1.98752 | C20-H23 | σ* | 0.00807 | 2.53 | 0.92 | 0.043 |
| C20-H21 | σ | 1.98785 | C17-H18 | σ* | 0.01787 | 2.53 | 0.91 | 0.043 |
| C20-H22 | σ | 1.98107 | O16-C17 | σ* | 0.03368 | 4.71 | 0.76 | 0.054 |
| C20-H23 | σ | 1.98858 | C17-H19 | σ* | 0.02080 | 2.44 | 0.91 | 0.042 |
| LP(1)O10 | n | 1.97758 | C2-C3 | σ* | 0.04126 | 6.46 | 1.13 | 0.076 |
| LP(2)O10 | n | 1.87048 | C1-C2 | π* | 0.34618 | 27.87 | 0.35 | 0.093 |
| LP(1)O12 | n | 1.97637 | C3-C4 | σ* | 0.02597 | 6.14 | 1.19 | 0.076 |
| LP(2)O12 | n | 1.88491 | C3-C4 | π* | 0.39872 | 25.84 | 0.36 | 0.093 |
| LP(1)O15 | n | 1.97760 | C6-C14 | σ* | 0.06520 | 2.64 | 1.11 | 0.049 |
| LP(2)O15 | n | 1.84822 | C6-C14 | σ* | 0.06520 | 17.32 | 0.69 | 0.100 |
| LP(2)O15 | n | 1.84822 | C14-O16 | σ* | 0.06520 | 32.02 | 0.63 | 0.128 |
| LP(1)O16 | n | 1.96486 | C14-O15 | σ* | 0.01716 | 6.74 | 1.17 | 0.080 |
| LP(2)O16 | n | 1.79886 | C14-O15 | π* | 0.26135 | 45.18 | 0.34 | 0.112 |
| C3-C4 | π* | 0.39872 | C1-C2 | σ* | 0.02157 | 205.92 | 0.02 | 0.082 |
| C3-C4 | π* | 0.39872 | C5-C6 | π* | 0.39299 | 194.65 | 0.02 | 0.083 |
| C14-O15 | π* | 0.26135 | C5-C6 | π* | 0.39299 | 155.02 | 0.01 | 0.073 |
| C14-O16 | σ* | 0.06520 | C17-H19 | σ* | 0.02080 | 1.71 | 0.04 | 0.031 |

[a]$E^{(2)}$ means energy of hyper conjugative interaction (stabilisation energy); [b]Energy difference between donor and acceptor i and j NBO orbitals; [c]F(i,j) is the Fork matrix element between i and j NBO orbitals.

TABLE-4
EXPERIMENTAL AND COMPUTED WAVENUMBERS CALCULATED FOR EDB MOLECULE BY B3LYP/6311G(d,p) METHOD

| Mode nos. | Experimental wavenumber ($cm^{-1}$) | | Computed wavenumber ($cm^{-1}$) | | | | PED (≥ 10%) assignments |
|---|---|---|---|---|---|---|---|
| | FT-IR | FT-Raman | Unscaled | Scaled | $IR_{Int}$ | $Ram_{Act}$ | |
| 1 | 3496 vs | 3509 vw | 3845 | 3717 | 98.433 | 155.399 | νOH (100) |
| 2 | 3427 m | | 3793 | 3667 | 103.210 | 74.748 | νOH (100) |
| 3 | 3265 br | 3266 vw | 3221 | 3114 | 0.698 | 72.218 | νCH (98) |
| 4 | | 3107 vw | 3211 | 3104 | 2.857 | 60.512 | νCH (100) |
| 5 | 3068 w | 3080 vw | 3155 | 3050 | 16.371 | 115.840 | νCH (98) |
| 6 | | | 3132 | 3028 | 27.335 | 7.720 | νCH (99) |
| 7 | | | 3111 | 3008 | 8.245 | 91.968 | νCH (97) |
| 8 | 2981 m | 2987w | 3098 | 2995 | 32.348 | 116.248 | νCH (100) |
| 9 | | 2971 m | 3070 | 2968 | 28.210 | 115.537 | νCH (94) |
| 10 | 2396 w | 2938 m | 3036 | 2935 | 20.778 | 165.275 | νCH (100) |
| 11 | 1682 vs | 1674 vs | 1774 | 1715 | 250.494 | 100.861 | νOC (85) |
| 12 | 1610 vs | 1614 vs | 1657 | 1602 | 60.946 | 133.031 | νCC (49) |
| 13 | 1558 w | | 1641 | 1587 | 45.688 | 2.961 | νCC (69) |
| 14 | 1515 ms | | 1544 | 1493 | 115.932 | 1.043 | βHCC (30) + νCC (15) |
| 15 | 1475 m | 1469 m | 1510 | 1460 | 16.063 | 4.193 | βHCH (70) |
| 16 | | | 1500 | 1450 | 12.500 | 29.859 | βHOC (17) + νCC (14) |
| 17 | | 1443 w | 1492 | 1442 | 8.861 | 14.878 | βHCH (82) |
| 18 | | | 1488 | 1439 | 13.570 | 24.208 | βHCH (84) |
| 19 | 1389 s | 1371 s | 1423 | 1376 | 9.670 | 1.302 | δCHCH (46) + δCHHH (36) |
| 20 | 1367 s | | 1401 | 1354 | 18.539 | 3.723 | δCHCH (26) + δCHHH (51) |
| 21 | 1336 m | | 1392 | 1346 | 13.118 | 8.241 | νCC (53) |
| 22 | | 1295 vs | 1345 | 1300 | 258.181 | 12.737 | βHOC (43) + βHCC (24) |
| 23 | 1291 m | | 1336 | 1292 | 0.706 | 7.941 | βHOC (79) |
| 24 | | | 1316 | 1272 | 448.613 | 56.006 | νOC (33) + νCC (25) |
| 25 | 1236 ms | 1244 vs | 1296 | 1253 | 127.637 | 24.006 | HCC (32) + νOC (14) + νCC (11) |
| 26 | 1188 m | | 1236 | 1195 | 254.453 | 30.310 | νOC (39) + νCC (10) |
| 27 | 1169 w | 1174w | 1212 | 1172 | 41.945 | 2.709 | βHOC (30) + βHCC (26) + νCC (12) |
| 28 | | | 1197 | 1157 | 23.991 | 1.740 | δCCOH (33) + δCHCH (33**)** |
| 29 | 1128 ms | 1130 vw | 1174 | 1135 | 55.543 | 2.270 | βHCC (41) + βHOC (31) + νCC (12) |
| 30 | 1096 ms | 1095 m | 1135 | 1097 | 280.452 | 2.688 | βHOC (17) + βCCC (15) + βHCC (13) |
| 31 | | | 1119 | 1082 | 47.270 | 4.612 | βHCC (40) + βCCO (14) + νCC (13) + νOC (10) |
| 32 | 1021 s | 1028 m | 1101 | 1064 | 23.833 | 5.842 | νCC (33) + νOC (10) + βHCC (10) |
| 33 | 956 s | 954 m | 1031 | 997 | 63.541 | 5.191 | νCC (38) + νOC (30) |
| 34 | 911 vs | | 948 | 917 | 46.273 | 4.560 | βCCC (16) + νCC (11) |
| 35 | | | 935 | 904 | 1.915 | 0.432 | δCCCH (77) + τHCCC (20) |
| 36 | 874 vs | 874 m | 914 | 884 | 12.861 | 0.592 | δCCCH (86) |
| 37 | 826 m | | 876 | 847 | 12.699 | 17.653 | νOC (27) + νCC (16) |
| 38 | 823 m | 824 w | 839 | 811 | 2.307 | 1.042 | δCHCH (14) + δCCOH (13) |
| 39 | 779 ms | 782 vs | 817 | 790 | 4.748 | 0.530 | τHCCC (50) + δOCOC (24) |
| 40 | 762 s | 776 vs | 792 | 766 | 39.560 | 18.440 | νCC (35) + νOC (20) |
| 41 | | | 778 | 752 | 2.496 | 9.829 | δCCOH (35) + δCHCH (13) + βCCO (10) |
| 42 | 721 m | | 769 | 743 | 55.125 | 1.921 | δOCOC (50) + τHCCC (13) + δCCCH (11) + τCCCC (10) |
| 43 | 666 m | | 703 | 680 | 2.115 | 0.094 | τCCCC (73) |
| 44 | 637 vs | 643 ms | 648 | 626 | 15.599 | 2.939 | βCCC (26) + νCC (10) |
| 45 | 589 m | | 591 | 571 | 12.404 | 6.812 | βCCO (50) + νCC (13) |
| 46 | 543 w | 540 ms | 584 | 565 | 0.324 | 0.107 | τCCCC (52) + τCCCO (27) |
| 47 | 528 m | | 538 | 520 | 2.319 | 0.639 | βCCC (37) + βCCO (24) |
| 48 | 451 m | 453 m | 461 | 446 | 3.990 | 0.412 | τCCCC (63) |
| 49 | 429 w | | 454 | 439 | 8.760 | 1.567 | βCCO (34) |
| 50 | 410 w | | 423 | 409 | 67.051 | 1.367 | τHOCC (83) |
| 51 | | | 398 | 385 | 9.120 | 0.989 | βCCO (27) + βCCC (27) |
| 52 | | 338 m | 346 | 335 | 3.142 | 1.739 | τCCCO (44) + βCOC (14) + τCCCC (13) |
| 53 | | | 332 | 321 | 7.503 | 0.974 | βCOC (26) + τCCCO (14) + τHCCO (13) |
| 54 | | 310 ms | 315 | 305 | 5.223 | 1.135 | βCCO (77) |
| 55 | | | 286 | 277 | 2.455 | 2.648 | βCCO (34) + νCC (17) |
| 56 | | 245 w | 251 | 243 | 140.643 | 1.979 | τHOCC (86) |

| | | | | | | |
|---|---|---|---|---|---|---|
| 57 | 226 w | 235 | 227 | 1.518 | 0.128 | τHCCO (74) + βCOC (11) |
| 58 | | 214 | 207 | 15.944 | 2.980 | τCCCO (46) + τCCCC (25)) |
| 59 | 157 w | 141 | 136 | 1.103 | 0.085 | βCCC (41) + βCCO (24) + τCOCC (11) |
| 60 | | 130 | 126 | 0.064 | 0.502 | τCCCC (41) + τCCOC (24) + τCCCO (20) |
| 61 | 87vs | 91 | 88 | 0.407 | 0.349 | τCOCC (50) + τCCCO (15) + τCCCC (14) |
| 62 | | 54 | 52 | 2.443 | 1.208 | τCCOC (57) + τCCCC (17) + τCOCC (10) |
| 63 | | 46 | 44 | 0.153 | 1.513 | τCCCO (73) + τCOCC (18) |

$IR_{int}$ = IR intensity; $Ram_{Int}$ = Raman activity; $Kmmol^{-1}$, w = weak; vw = very weak; s = strong; vs = very strong; m = medium; br = broad, sh = shoulder, υ = stretching; δ = in plane bending ; γ = out-of-plane bending; τ = torsion.

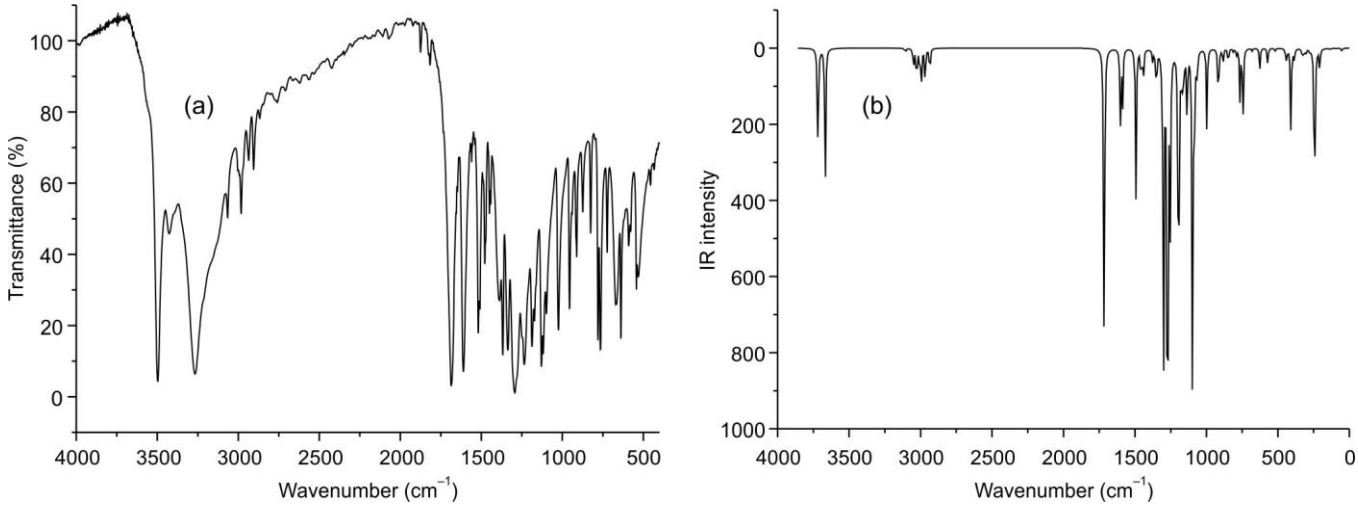


Fig. 3 (a). Experimental FT-IR and (b) constructed FT-IR spectrum for EDB molecule

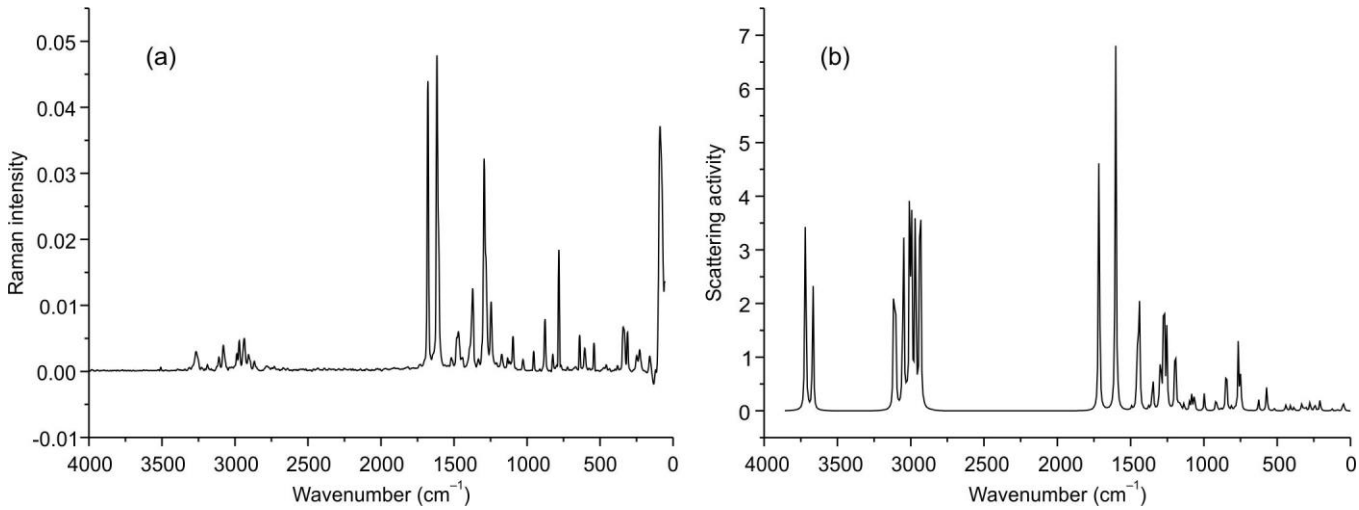


Fig. 4. (a) Experimental FT-Raman and (b) constructed FT-Raman spectrum for EDB molecule

in both FT-IR and FT-Raman spectrum are assigned to C–H out-of-plane bending vibrations with PED contribution of ~ 70% in the PED column. The wavenumbers for the mode in 904, 884 and 752 $cm^{-1}$ (mode nos. 35, 36 and 41) by B3LYP/ 6-311G(d,p) method as shown in Table-4.

**O–H vibrations:** The O–H stretching in the molecules are very sensitive to hydrogen bonding. In case of non-hydrogen bond or free O–H group found between 3600-3550 $cm^{-1}$ region. If hydrogen bond exists in the molecule it falls between 3550-3200 $cm^{-1}$ region [31,32]. The EDB molecule have two hydroxyl group (O12-H13 and O10-H11) the O–H stretching vibrations shows are very strong and one medium band at 3496 and 3427 $cm^{-1}$. The scaled wavenumbers at 3717, 3667 $cm^{-1}$ (mode nos. 1 and 2) are assigned to O–H stretching vibrations and also note that this O–H group seems to be free stretching vibrations as evident from PED contribution of 100%. The deviation happens between computed and recorded spectral data may be due to inter molecular hydrogen bonding formation in the EDB molecule. The in-plane bending mode of O–H group appear near 1440-1260 $cm^{-1}$ in the FT-IR spectrum [29,33].

The computed O–H in-plane bending mode decreases at 1292 and 1450 $cm^{-1}$ (mode no. 16 and 23) by B3LYP/6-311G-(d,p) method coincide with recorded FT-IR spectrum at 1291

$cm^{-1}$. The O–H out-of-plane bending vibration is generally reported near 312 and 280 $cm^{-1}$ for free hydroxyl groups, whereas associated hydroxyl groups exhibit bands around 612 and 557 $cm^{-1}$ [34]. In present study, these vibrations were observed at 410 $cm^{-1}$ in the FT-IR spectrum and 245 $cm^{-1}$ in the FT-Raman spectrum. The corresponding calculated frequencies were obtained at 409 and 243 $cm^{-1}$ (mode nos. 50 and 56), respectively. These modes show PED contributions of approximately 85%, confirming their assignment to O–H out-of-plane bending vibrations, as shown in Table-4

**C=O and C–O vibrations:** The carbonyl stretching vibration (C=O) is generally observed in the region of 1715-1680 $cm^{-1}$ [35]. In the EDB molecule, a strong band was recorded at 1682 $cm^{-1}$ in the FT-IR spectrum and at 1674 $cm^{-1}$ in the FT-Raman spectrum, corresponding to the C14=O15 stretching vibration. The corresponding theoretical frequency was calculated at 1715 $cm^{-1}$ (mode no. 11) with a PED contribution of 85%, confirming its assignment. The C=O in-plane bending vibration is typically identified in the range of 820-630 $cm^{-1}$ [36]. In this case, this mode was observed as a medium-intensity band at 528 $cm^{-1}$ and calculated at 520 $cm^{-1}$ (mode no. 47) with a PED contribution of 24%. The C=O out-of-plane bending mode was also identified from the recorded and calculated spectra, as listed in Table-4.

The EDB molecule contains two C–O bonds associated with hydroxyl groups and two C–O bonds connecting the ester and ethyl moieties. The C–O stretching vibrations were calculated at 1272, 1195 and 997 $cm^{-1}$ (mode nos. 24, 26 and 33), while the corresponding experimental bands were observed at 1188 and 956 $cm^{-1}$ in the FT-IR spectrum and at 954 $cm^{-1}$ in the FT-Raman spectrum. The C–O in-plane bending vibrations generally occur in the 460-175 $cm^{-1}$ region and were calculated at 385, 321, 305, 277, 227 and 136 $cm^{-1}$ (mode nos. 51, 53, 54, 55, 57 and 59). These assignments are supported by the FT-Raman bands observed at 310, 226 and 157 $cm^{-1}$, which correlate well with the computed frequencies.

**$CH_2$ and $CH_3$ group vibrations:** The $CH_2$ group have six fundamental mode of vibrations namely, symmetric and antisymmetric stretching, scissoring, rocking, twisting and wagging. The $CH_2$ stretching vibration expect 3000-2800 $cm^{-1}$ or in other words, asymmetric and symmetric band expect in 3000-2900 $cm^{-1}$ and 2900 and 2800 $cm^{-1}$ [36]. In FT-Raman spectrum at 2971 $cm^{-1}$ indicate the $CH_2$ symmetric vibration. The wavenumber computed for $CH_2$ symmetric mode is 2968 $cm^{-1}$ (mode no. 9) by B3LYP/6-311G(d,p) method. The computed wavenumber at 3028 $cm^{-1}$ are assigned to $CH_2$ asymmetric stretching vibrations. The $CH_2$ bending identified from wavenumber 845-450 $cm^{-1}$ [37]. The $CH_2$ scissoring mode computed at 811 $cm^{-1}$ (mode no. 38) by B3LYP/6-311G(d,p) method, the recorded FT-IR and FT-Raman wavenumber are at 824 and 823 $cm^{-1}$ are assigned to $CH_2$ scissoring mode. The other $CH_2$ vibration as rocking, twisting and wagging vibrations are falls in the respective vibrational wavenumber as evident from Table-4. Normally, methyl ($CH_3$) or electron donating group and have nine fundamental mode of vibrations. The $CH_3$ asymmetric and symmetric vibrations falls around 3000-2840 $cm^{-1}$ [38]. The $CH_3$ anti-symmetric and symmetric vibrations for EDB molecule is computed for 2995, 3008 and 2935 $cm^{-1}$ (mode no. 8, 7, 10) by B3LYP/6-311G(d,p) method recorded spectrum at 2981, 2936 $cm^{-1}$ in FT-IR spectrum and 2987, 2938 $cm^{-1}$ in FT-Raman are assigned to $CH_3$ asymmetric and symmetric stretching vibrations. The antisymmtric and symmetric deformation of the $CH_3$ group is falls in the range 1465-1440 $cm^{-1}$ and 1040-990 $cm^{-1}$ [39]. The computed antisymmetic and symmetric deformation at 1460 $cm^{-1}$ (mode no. 15) and 904 $cm^{-1}$ (mode no. 35) by B3LYP/6-311G(d,p) method the recorded FT-IR and FT-Raman spectral wavenumber at 1475 $cm^{-1}$ and 1469 $cm^{-1}$ are assigned to symmetric deformation of methyl group.

**Ring vibrations:** Normally ring system contain only carbon atoms, the ring C–C stretching falls near 1625-1430 $cm^{-1}$ reported by Varsanyi [29]. The calculated wavenumbers at 1602, 1587, 1493, 1450, 1346, 1272, 1253 $cm^{-1}$ (mode nos. 12, 13, 16, 14, 21, 24, 25). The recorded FT-IR wavenumber for the C–C stretching mode 1610, 1558, 1515, 1336, 1236 $cm^{-1}$ and in 1614, 1244 $cm^{-1}$ are assign to C–C stretching vibration in aromatic ring system. The other vibrations namely C–C–C in-plane and C–C–C out-of-plane bending mode are shown in Table-4.

**UV-Vis spectral and FMO analysis:** The recorded UV-Vis spectrum of EDB molecule was measured using ethanol as solvent as shown in Fig. 5a-b along with constructed spectrum. The recorded $\lambda_{max}$ wavelength was found at 295 nm, at the same time the TD-DFT/B3LYP/6-311G(d,p) method predict 278.02 nm in ethanol phase and 273.61 nm in gas phase are shown in Table-5. The deviation between the experimental and theoretical wavelength is ~15 nm. This may be due to solvent effect and lack of solvent-solute interactions. The first transition corresponds to HOMO→LUMO contribution of 84%. The corresponding contribution for the transition is n→π*. The HOMO-LUMO orbital contribution play important role in chemical reaction, The HOMO represent ability to give electron where LUMO have ability to accept electrons [40].

TABLE-5
THE COMPUTED AND EXPERIMENTAL UV-VIS DATA BY TD-DFT METHOD AT B3LYP/6-311G(d,p) METHOD

| λ (nm) | E (eV) | Computed (wavelength) | (f) | Expt. (ethanol) (wavelength) | Major contribution | Assignment |
|---|---|---|---|---|---|---|
| Gas | 4.5314 | 273.61 | 0.0958 | | H→L (80%) | n→π* |
| | 4.9976 | 248.09 | 0.0002 | | H-2→L (96%) | π→π* |
| | 5.1199 | 242.16 | 0.1168 | | H-1→L (48%), H→L (14%), H→L+1 (37%) | π→π* |
| Ethanol | 4.4595 | 278.02 | 0.1543 | 295 | H→L (84%) | n→π* |
| | 5.0139 | 247.28 | 0.1501 | | H-1→L (55%), H→L (11%), H→L+1 (32%) | π→π* |
| | 5.1333 | 241.53 | 0.0004 | | H-2→L (96%) | π→π* |

[a]H-HOMO; L-LUMO

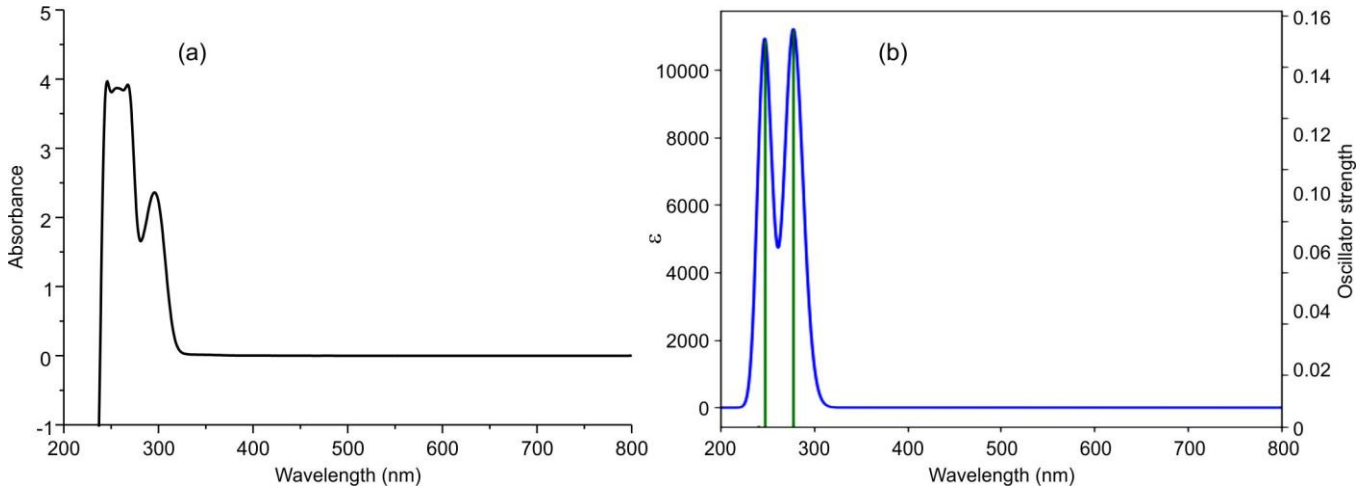


Fig. 5. (a) UV-Vis spectrum of EDB compound (b) contracted UV-Vis spectrum of EDB

Frontier molecular orbitals (FMOs) play a significant role in determining the electronic, optical, and chemical properties of molecular systems and are widely used to interpret charge-transfer behaviour and electronic transitions observed in UV-Vis spectra [41]. The energies of the HOMO and LUMO provide valuable information regarding the chemical reactivity, kinetic stability and intramolecular charge-transfer (ICT) characteristics of a molecule [42,43]. In the present study, the HOMO and LUMO energies were calculated to be -6.17 and -1.15 eV, respectively, resulting in an energy gap of 5.02 eV. The relatively large HOMO–LUMO gap suggests good molecular stability and moderate chemical reactivity of the EDB molecule.

The energy difference indicates charge delocalisation happen while transition. The band gap energy difference for first three electronic states in solvent phase are 4.495 eV, 5.013 eV and 5.133 eV correlate with the HOMO-LUMO energy gap. The important ionisation potential (I) = $-E_{HOMO}$, electron affinity (A) = $-E_{LUMO}$ are 6.17 and 1.15 eV the electronegativity, chemical hardness, chemical softness, chemical potential and Electrophilicity index are shown in Table-6. The HOMO-LUMO diagram along with band gap is shown with density of state (DOS) spectrum are shown in Fig. 6. It is worth to mention chemical hardness is the good indicator for chemical stability. The calculated chemical hardness ($\eta$ = 2.51 eV) indicates good molecular stability, while the softness (S = 0.19 $eV^{-1}$) suggests low polarizability and moderate reactivity, consistent with the HOMO–LUMO energy gap.

**TG/DTA analysis:** The thermal behaviour and decomposition pattern of EDB were investigated using thermogravimetric (TG) and differential thermal (DTA) analyses, and the results are shown in Fig. 7. The TG curve reveals a negligible mass loss below 130 ºC, which can be attributed to the removal of moisture and trace volatile impurities. The compound remains thermally stable up to approximately 200 ºC. Beyond this temperature, a major weight loss is observed, indicating the onset of thermal decomposition. This degradation process is primarily associated with the cleavage of the ester group (–COOEt), followed by the decomposition of the phenolic moiety. At higher temperatures, further mass loss occurs due to the carbonization of the remaining organic fragments.

TABLE-6
HOMO–LUMO ENERGIES AND CALCULATED GLOBAL REACTIVE PARAMETERS OF EDB MOLECULE COMPUTED BY B3LYP/6-311G(d,p) METHOD

| Parameters | B3LYP/6-311G(d,p) |
|---|---|
| | Gas phase |
| $E_{HOMO}$ (eV) | -6.17 |
| $E_{LUMO}$ (eV) | -1.15 |
| $E_{HOMO} - E_{LUMO}$ (eV) | 5.02 |
| Ionisation potential (I) | 6.17 |
| Electron affinity (A) | 1.15 |
| Electronegativity ($\chi$) | 3.66 |
| Chemical hardness ($\eta$) | 2.51 |
| Chemical softness (S) | 0.19 |
| Chemical potential ($\mu$) | -5.66 |
| Electrophilicity index ($\omega$) | 6.38 |

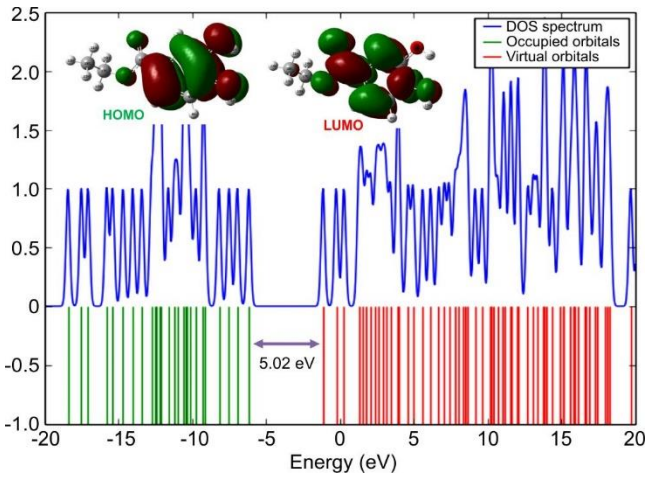


Fig. 6. Density of state (PDOS) spectrum of EDB

The DTA curve exhibits a weak endothermic peak in the range of 130-140 ºC, corresponding to the melting of the compound. A prominent exothermic peak above 200 ºC is attributed to ester bond cleavage and subsequent fragmentation of the aromatic framework. These TG/DTA results suggest that EDB undergoes a single major decomposition pathway involving ester-group degradation followed by aromatic-ring fragmentation.

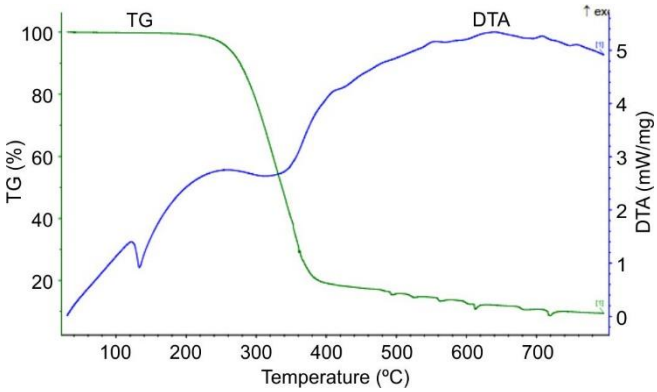


Fig. 7. TG/DTA spectrum of ethyl 3,4-dihydroxybenzoate

**Molecular electrostatic potential (MEPs) analysis:** The MEP analysis provide details about electrophilic and nucleophilic site in the molecular reaction and it also determine the presence of hydrogen bonding [44]. The expression for the MEP value was calculated as follows [45]:

$$v(r)\sum NA[Za]|r - R_A| - \int \rho(r')|r - r'|$$

where N denote total number of nuclei, $Z_a$ denote charge of nucleus, kept at $R_A$, ρ(r′) denote electron density function of molecule, r′ is the dummy integration. In EDB molecule the MEP diagram was drawn using Gauss View 5.08 [10] software as shown in Fig. 8.

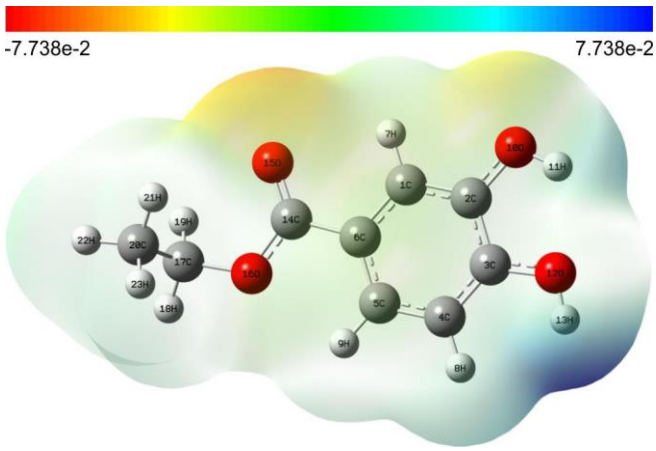


Fig. 8. MEP diagram of EDB molecule

The potential increase in order from blue to red. The negative region (red, orange and yellow) denote electrophilic site. The positive region denotes nucleophilic site denote by blue colour. The molecular electrostatic potential (MEP) map (Fig. 8) shows negative potential regions (red) localized around the hydroxyl and carbonyl oxygen atoms, indicating electron-rich sites. Positive potential regions are distributed over the $CH_2$, $CH_3$ and aromatic hydrogen atoms, identifying the electrophilic regions of the EDB molecule.

**Electron–hole distribution analysis:** The nature of electronic excitation in the EDB molecule was further investigated through electron–hole analysis based on the TD-DFT calculations at the B3LYP/6-311G(d,p) level. The transition parameters for the first three excited states were computed using Multiwfn software [16] and the results are summarized in Table-7. The calculated parameters include excitation energy, electron–hole centroid distance (Δr), charge-transfer length (D) and electron–hole overlap integral (S). In the electron–hole distribution plots, electrons and holes are represented by green and blue colors, respectively. The Δr value reflects the extent of electron–hole separation and depends on their spatial overlap. Among the three excited states, the second excited state exhibits the largest Δr value of 2.2025 Å, followed by the first excited state (1.3888 Å) and the third excited state (1.0409 Å). Similarly, the charge-transfer lengths (D) were calculated as 1.6741, 1.3274 and 1.2159 Å for the second, first and third excited states, respectively. The electron–hole distribution maps (Figs. 9a-b) reveal significant electron delocalization during electronic excitation, while the overlap plots indicate considerable electron–hole interaction, supporting the charge-transfer character of the excited states.

TABLE-7
CHARGE TRANSFER LENGTH, Δr, OVERLAP INTEGRAL, FOR FIRST THREE EXCITED STATE EDB MOLECULE

| Excited state | Electron–hole (S) overlap integral | Δr (Å) | Charge transfer length (D) (Å) | Excitation energy (E) eV |
|---|---|---|---|---|
| 1 | 0.5130 | 1.3888 | 1.3274 | 4.531 |
| 2 | 0.2118 | 2.2025 | 1.6741 | 4.998 |
| 3 | 0.5807 | 1.0409 | 1.2159 | 5.120 |

**Reduced density gradient (RDG) analysis:** Reduced density gradient (RDG) analysis is an extension of the atom-in-molecules (AIM) approach and provides a visual description of weak non-covalent interactions within molecular systems [16]. The RDG isosurfaces and corresponding scatter plot for the EDB molecule are shown in Fig. 10a. The analysis is based on the electron density (ρ) and the sign of the second eigenvalue of the Hessian matrix, sign($\lambda_2$)ρ, which enables the identification of different types of intermolecular interactions. In general, sign($\lambda_2$)ρ < 0 corresponds to attractive interactions, sign($\lambda_2$)ρ > 0 indicates steric repulsion, and values close to zero are associated with weak van der Waals (vdW) interactions [46]. As shown in Fig. 10b, the red region within the aromatic ring represents strong steric repulsion, whereas the green isosurfaces correspond to weak vdW interactions. These interactions are mainly associated with O–H···O–H and C=O···H contacts involving the oxygen-containing functional groups. The predominance of green and blue regions in the RDG map suggests the presence of significant non-covalent interactions, which contribute to the overall stabilization of the EDB molecule [47].

**Wavefunction (ELF and LOL) analysis:** The electron localization function (ELF) and localized orbital locator (LOL) analyses were performed using the Multiwfn program [16] to investigate the electron localization and bonding characteristics of the EDB molecule. The corresponding 2D and 3D maps are shown in Figs. 11a-b and 12a-b. These analyses provide information about the probability of finding electron pairs and are useful for understanding the covalent bonding nature within the molecule. Since both ELF and LOL are based on the kinetic energy density of electrons, they exhibit similar chemical mapping behaviour [48].

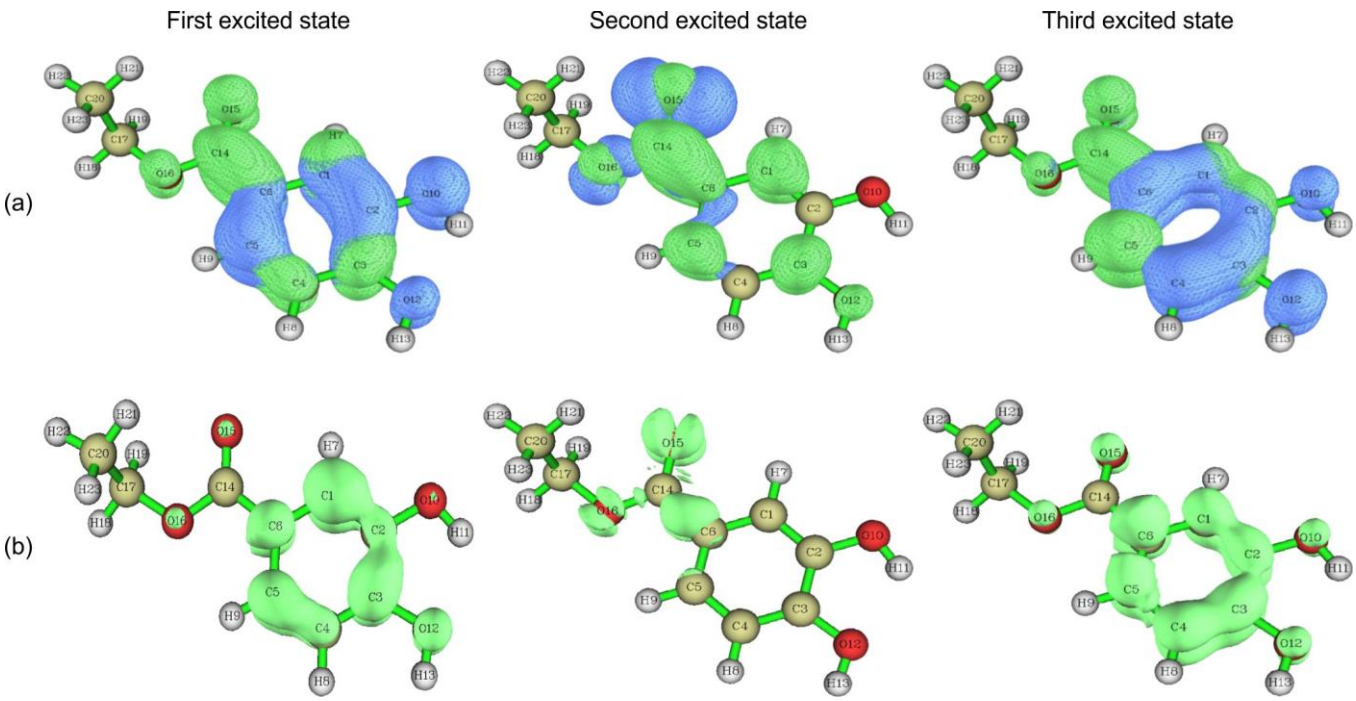


Fig.9. (a) Electron-hole distribution and (b) electron-hole overlap for three excited states of EDB molecule

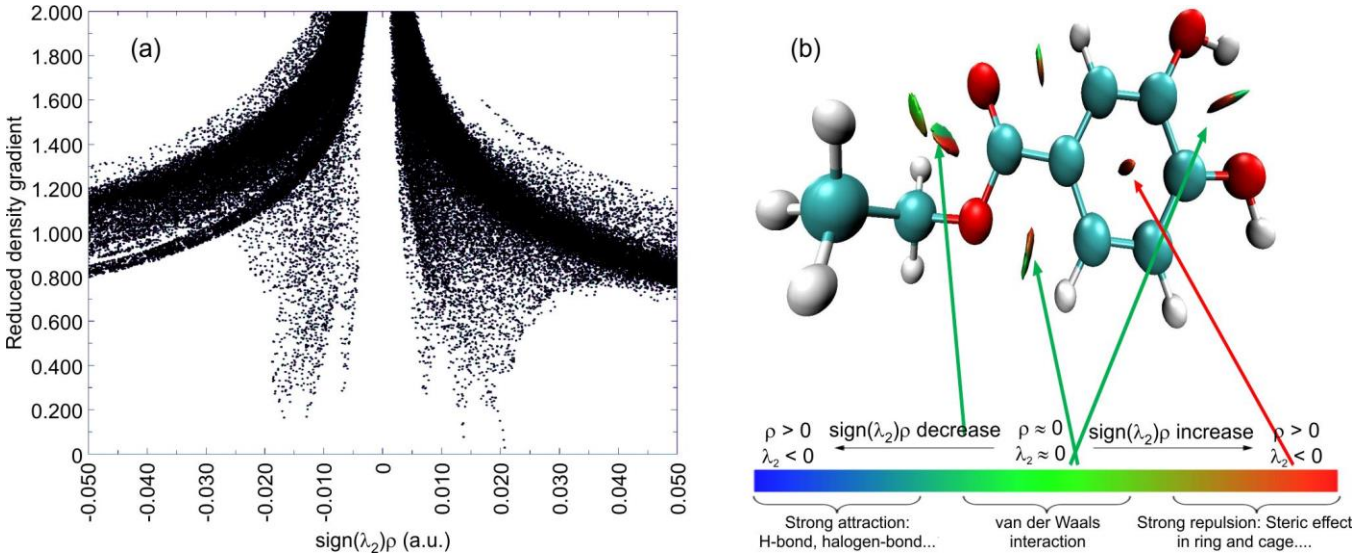


Fig. 10. (a) Scattering map and (b) reduced density gradient (RDG) for EDB molecule

The ELF maps of EDB (Figs. 11a-b) display characteristic relief patterns in which the atomic nuclei appear as distinct peaks. The ELF values range from 0 to 1, where values below 0.5 indicate electron delocalization, while values approaching 1 correspond to highly localized electron density [49]. Significant electron localization is observed around the oxygen atoms and along the C–O, C=O, and O–H bonds, confirming their strong covalent character. The lone-pair electrons of the oxygen atoms are also clearly distinguished as highly localized regions.

The LOL maps (Figs. 12a-b) further support these observations. Regions with LOL values greater than 0.5 indicate enhanced electron localization and are mainly associated with the electronegative oxygen atoms, represented by red regions of high electron density. In contrast, blue regions surrounding the nuclei correspond to electron-depleted zones between the inner and valence shells. Thus, the ELF and LOL analyses reveal substantial electron localization around the oxygen containing functional groups, highlighting their influence on the electronic structure and chemical reactivity of the EDB molecule [49].

**Drug likeness:** The drug-likeness properties of the EDB molecule were evaluated using various pharmacokinetic filters and the results are summarized in Table-8. Lipinski's rule of five is widely employed to assess the suitability of a compound as a potential drug candidate based on its physicochemical properties [50]. The EDB molecule satisfies the Lipinski, Veber, Egan and Ghose criteria indicating favour-

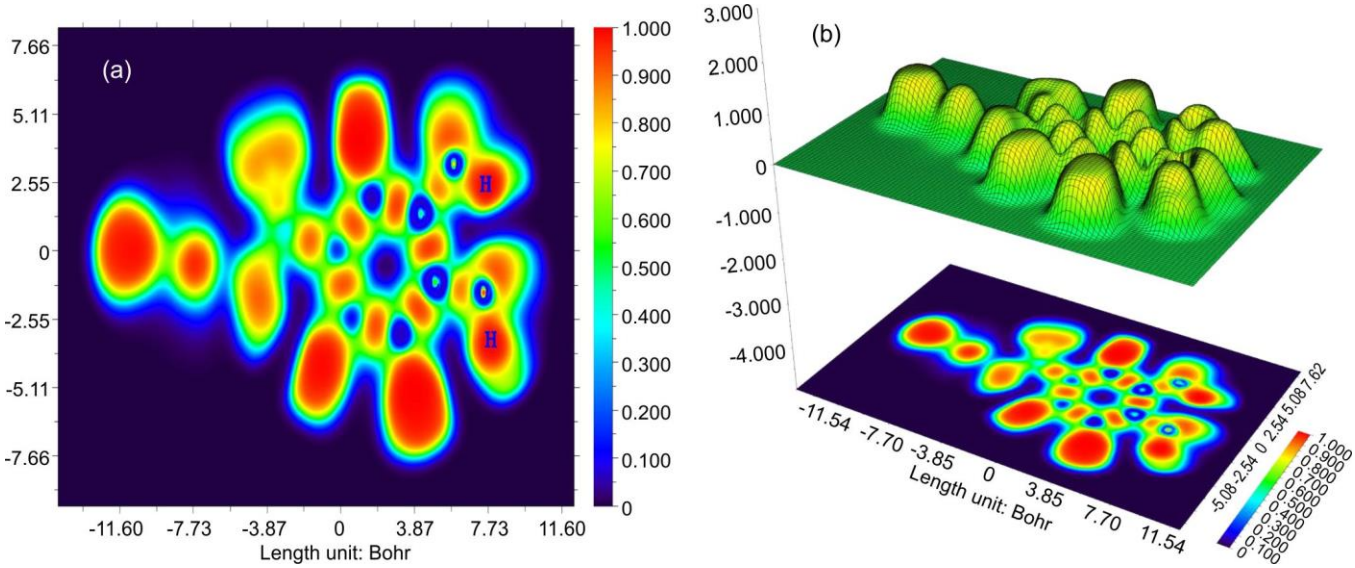


Fig. 11. (a) 2D ELF and (b) 3D ELF map of EDB molecule

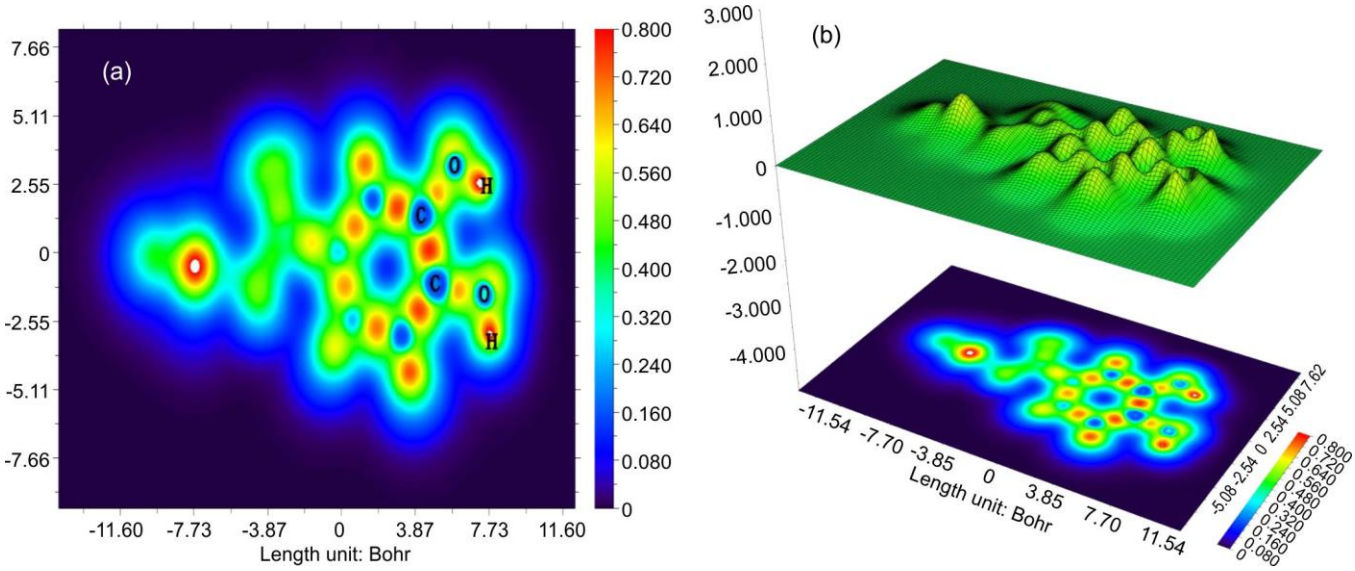


Fig. 12. (a) 2D LOL and (b) 3D LOL map of EDB molecule

able drug-like characteristics. According to Lipinski's rule, the numbers of hydrogen bond donors (HBD) and hydrogen bond acceptors (HBA) should be less than 5 and 10, respectively, while the molecular weight should be below 500 g/mol. For EDB, the HBD and HBA values are 2 and 4, respectively, and the molecular weight is 182.17 g/mol. In addition, the molar refractivity falls within the recommended limit of less than 140 $Å^3$ [51].

The PASS prediction results (Table-9) indicate that EDB possesses diverse biological activities, with high Pa values (> 0.90) for several enzyme inhibitory functions. Notably, EDB exhibited predicted anticancer activity against breast cancer (Pa = 0.216) and lung cancer (Pa = 0.151), supporting its selection for molecular docking and *in vitro* cytotoxicity studies.

Pharmacokinetic analysis further revealed high gastrointestinal (GI) absorption, suggesting good oral bioavailability. The BOILED-Egg model (Fig. 13a) places EDB within the yellow yolk region, indicating its potential ability to penetrate the blood–brain barrier (BBB), an important property for central nervous system (CNS) drug candidates [52,53]. The topological polar surface area (TPSA) of 66.76 $Å^2$ and WlogP value of 1.27 indicate a favourable balance between membrane permeability and aqueous solubility [54,55]. Furthermore, the predicted CYP1A2, CYP2C19, CYP2C9, CYP2D6 and CYP3A4 inhibition profiles suggest a low risk of metabolic complications [56]. The bioavailability radar plot (Fig. 13b) further confirms the favourable drug-like profile of EDB.

**Antibacterial activity study:** The antibacterial activity of EDB was evaluated against *S. aureus*, *E. coli*, *Shigella* sp., *P. aeruginosa* and *A. faecalis* using the agar well-diffusion method [57]. The compound was tested at concentrations of 10, 50 and 100 µL, with levofloxacin serving as the reference standard. Antibacterial efficacy was assessed by measuring the diameter of the inhibition zone (mm) and the results are shown in Table-10. It is found that the inhibition zone increased with

TABLE-8
DRUG LIKENESS AND PHYSICO-CHEMICAL PARAMETERS FOR PBD MOLECULE

| Descriptor | Value | Expected range |
|---|---|---|
| Number of hydrogen bond acceptor | 4 | < 10 |
| Alog P | 1.27 | < 5 |
| Number of hydrogen bond donor | 2 | < 5 |
| Molar refractivity | 46.57 | 40-130 |
| Molecular weight (g/mol) | 182.17 | < 500 |
| Number of rotatable bonds | 3 | < 10 |
| Topological polar surface area (Å$^2$) | 66.76 | < 140 |
| Number of heavy atoms | 13 | |
| Lipinski | yes | |
| Veber | yes | |
| Egan | yes | |
| Ghose | yes | |
| Muegge | No; 1 violation | |
| Bioavailability score | 0.55 | |
| Synthetic accessibility | 1.57 | |
| Pharmacokinetics | | |
| Consensus Log $P_{o/w}$ | 1.40 | |
| POLAR (polarity) | Polar | |
| GI absorption | High | |
| BBB permeant | yes | |
| CYP1A2 inhibitor | no | |
| CYP2C19 inhibitor | no | |
| CYP2C9 inhibitor | no | |
| CYP2D6 inhibitor | no | |
| CYP3A4 inhibitor | no | |
| Log Kp (skin permeation) | -6.10 cm/s | |

increasing concentration, indicating concentration-dependent antibacterial activity against all tested bacterial strains [57].

**Minimum inhibitory concentration (MIC):** The MIC values recorded for *S. aureus*, *E. coli*, *P. aeruginosa* found upto 50 µg/mL, whereas MIC exhibited for *Shigella* sp., *A. faecalis* around 75 µg/mL as shown in Table-11.

TABLE-9
PASS PREDICTION OF EDB COMPOUND

| Pa | Pi | Predicted activity |
|---|---|---|
| 0.926 | 0.002 | Arylsulfate sulfotransferase inhibitor |
| 0.925 | 0.004 | Chlordecone reductase inhibitor |
| 0.923 | 0.005 | Aspulvinone dimethylallyltransferase inhibitor |
| 0.922 | 0.006 | Membrane integrity agonist |
| 0.335 | 0.053 | Cancer associated disorders treatment |
| 0.251 | 0.084 | Antineoplastic (small cell lung cancer) |
| 0.216 | 0.086 | Antineoplastic (breast cancer) |
| 0.160 | 0.111 | Antineoplastic (endocrine cancer) |
| 0.151 | 0.100 | Antineoplastic (lung cancer) |
| 0.104 | 0.016 | Breast cancer-resistant protein inhibitor |

TABLE-10
ANTIBACTERIAL ACTIVITY OF EDB COMPOUND AT DIFFERENT CONCENTRATION AGAINST DIFFERENT BACTERIA

| Test organism | Control (levofloxacin) (mm) | Extract (mm) | | |
|---|---|---|---|---|
| | | 10 µL | 50 µL | 100 µL |
| *Staphylococcus* | 38 | 10 | 20 | 28 |
| *Escherichia coli* | 38 | 12 | 22 | 28 |
| *Shigella sp* | 36 | Nil | 10 | 22 |
| *Pseudomonas* | 38 | 10 | 20 | 28 |
| *Alcaligens faecalis* | 38 | Nil | 20 | 28 |

**Molecular docking analysis:** Molecular docking analysis was performed to evaluate the binding affinity and interaction pattern of EDB with the selected breast cancer (5TWZ) and lung cancer (5C5S) protein targets. The docking results revealed binding energies of -4.38 kcal/mol for 5TWZ and -3.32 kcal/mol for 5C5S, indicating a stronger interaction of EDB with the breast cancer target (Table-12). For the 5TWZ protein, EDB formed five hydrogen bonds involving residues GLU106, GLU106, SER233, SER236 and ARG103, with bond lengths of 2.1, 2.4, 2.4, 2.3 and 2.5 Å, respectively (Table-13). In contrast, the 5C5S protein exhibited three hydrogen-

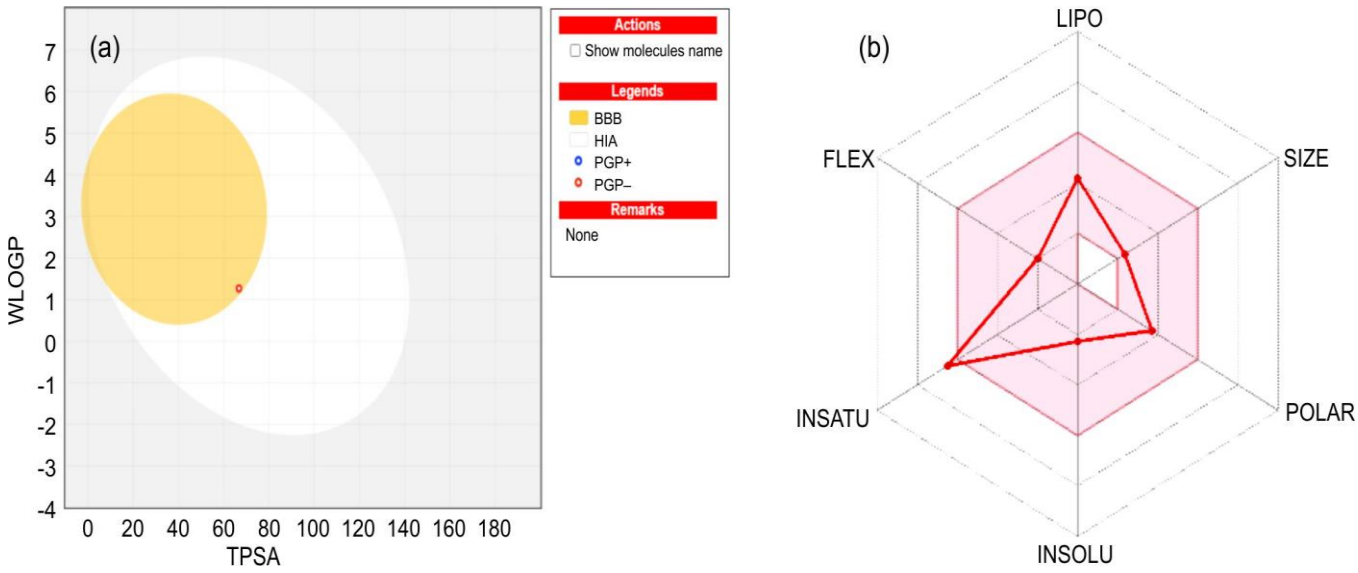


Fig. 13. (a) BOILED-Egg diagram for 234THB compound including the referenced drug and (b) bioavailability radar chart for EDB compound

TABLE-11
MINIMUM INHIBITORY CONCENTRATION (MIC)

| Test organisms | Minimal inhibitory concentration (µg/mL) | | | | | |
|---|---|---|---|---|---|---|
| | 10 | 25 | 50 | 75 | 100 | C |
| *Staphylococcus aureus* | + | + | (MIC) | – | – | – |
| *Escherichia coli* | + | + | (MIC) | – | – | – |
| *Shigella* sp. | + | + | + | (MIC) | – | – |
| *Pseudomonas aeruginosa* | + | + | (MIC) | – | – | – |
| *Alcaligens faecalis* | + | + | + | (MIC) | – | – |

+ Turbidity (growth), – No turbidity (no growth), C – control uninoculated broth MIC – No growth (minimal inhibitory concentration).

TABLE-12
MOLECULAR DOCKING RESULTS OF
EDB MOLECULE WITH CANCER TARGET

| Compound | Protein (ID) | Binding energy (Kcal/mol) | Inhibition constant Ki (µM) | RMSD |
|---|---|---|---|---|
| EDB | 5TWZ | -4.38 | 615.90 | 27.36 |
| | 5C5S | -3.32 | 3.66 | 61.55 |

bond interactions with residues GLU231, GLU231 and HIS238, having bond distances of 2.0, 2.3 and 2.1 Å, respectively (Fig. 14a-b). Since all hydrogen-bond lengths are less than 3 Å, these interactions can be considered strong and contribute

TABLE-13
SUMMARY OF HYDROGEN BONDING OF
EDB MOLECULE WITH CANCER TARGET

| Protein | No. of hydrogen bond formed | Bonded Residues | Bond length |
|---|---|---|---|
| 5TWZ | 5 | Protein: A: GLU 106 | 2.1 |
| | | Protein: A: GLU 106 | 2.4 |
| | | Protein: A: SER 233 | 2.4 |
| | | Protein: A: SER 236 | 2.3 |
| | | Protein: A: ARG 103 | 2.5 |
| 5C5S | 3 | Protein: A: GLU 231 | 2.0 |
| | | Protein: A: GLU 231 | 2.3 |
| | | Protein: A: HIS 238 | 2.1 |

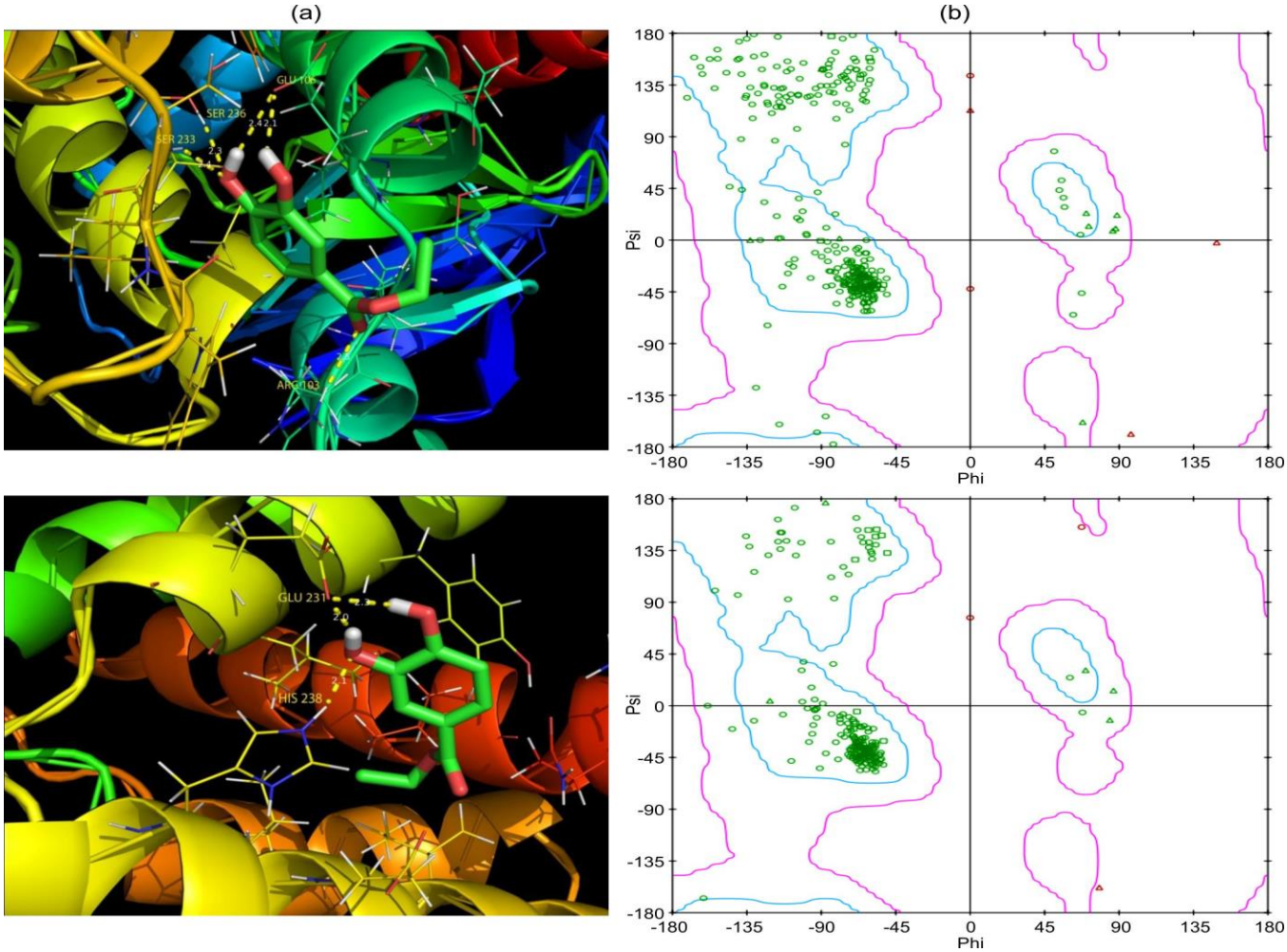


Fig. 14. Protein-ligand in 3D form for protein (a) ID: 5TWZ, ID: 5C5S and (b) Ramachandra plot

significantly to the stability of the protein–ligand complexes. The larger number of hydrogen bonds and more favourable binding energy observed for the 5TWZ complex suggest a relatively stronger binding affinity of EDB toward the breast cancer target. Furthermore, the Ramachandran plots (Fig. 14a-b) indicate that the interacting residues are located within the allowed regions, supporting the structural reliability and stability of the docked protein-ligand conformations [58].

**MTT assay:** The cytotoxic effect of EDB was assessed against human lung cancer cell line (A549) and breast cancer cell line (MCF 7). After 24 h of treatment, EDB reduced the viability of both A549 and MCF-7 cells in a concentration-dependent manner, with $IC_{50}$ values of 30.78 µg/mL and 27.44 µg/mL, respectively, indicating slightly greater activity against MCF-7 cells. The concentration *vs*. cell inhibition of lung and breast cancer protein are shown in Fig. 15. Figs. 16a-f and 17a-f clearly indicated that the varying concentration (6.5, 12.5, 25, 50 and 100 µg/mL) of EDB treatment was significantly inhibit the proliferation of A 549 and MCF-7 cells in a dose dependent manner. Among the two cancer cell lines EDB have best activity on breast cancer cell lines are observed. Significantly, EDB exhibited best activity against the MCF-7 breast cancer line compared to the A 549 lung cancer line.

## Conclusion

The structural and vibrational analyses performed at the B3LYP/6-311G(d,p) level confirmed the presence of the characteristic functional groups and aromatic framework of ethyl 3,4-dihydroxybenzoate (EDB) molecule. The calculated geometric parameters showed excellent agreement with the available XRD data. The C=O and C–O bond lengths were also consistent with reported literature values. The O–H stretching vibrations indicate the presence of strong hydrogen-bonding interactions in the EDB molecule. Furthermore, the C–H, O–H and C=O stretching modes were identified as nearly pure vib-

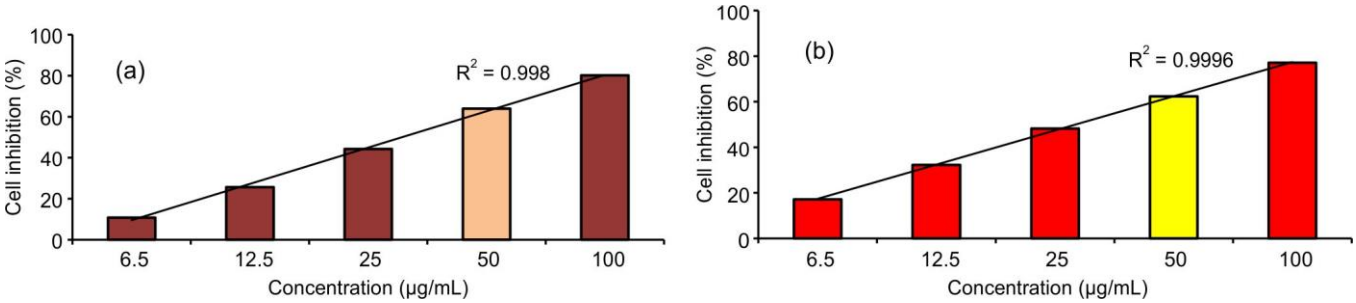


Fig. 15. Graph between concentration *vs*. cell inhibition of (a) lung cancer and (b) breast cancer cell line

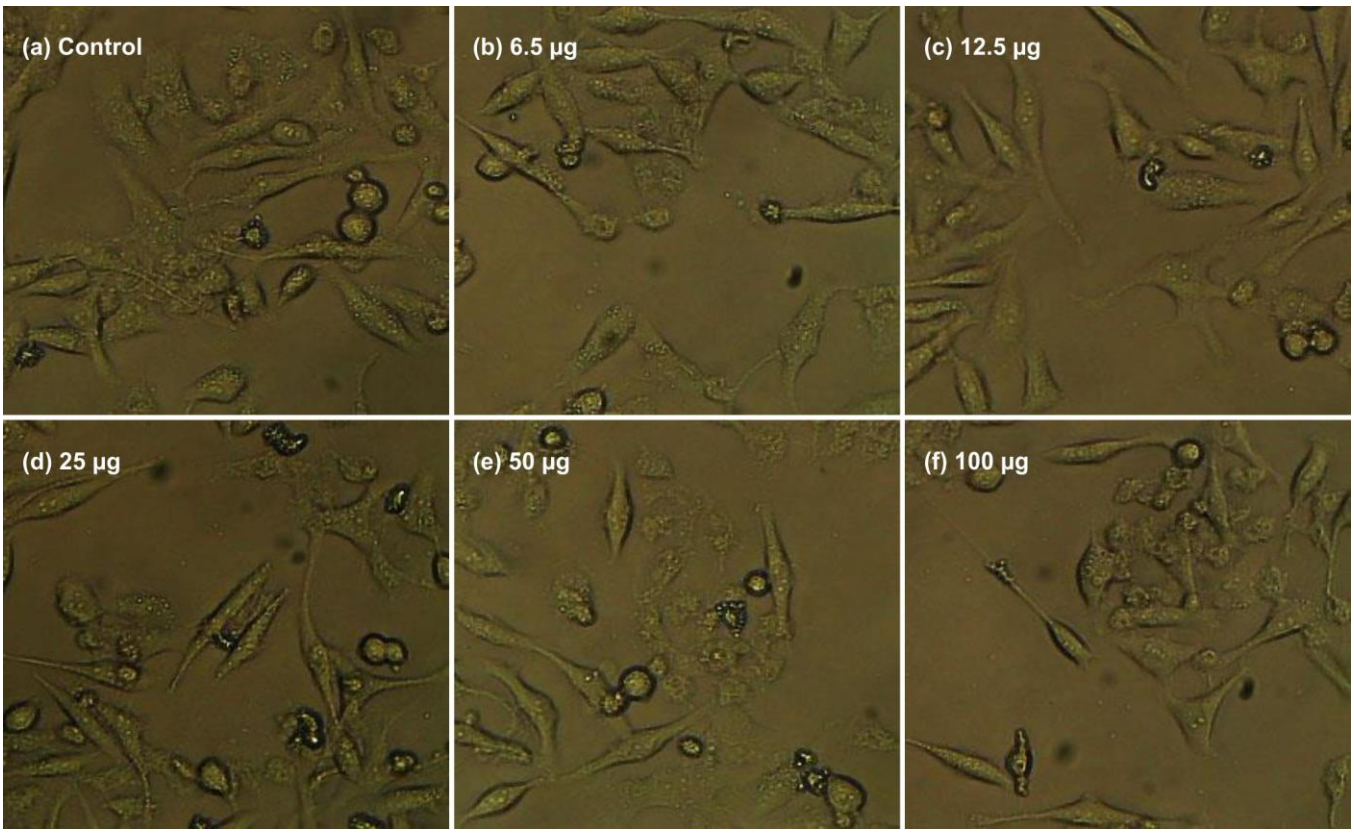


Fig. 16. Anticancer activity of lung cancer (A549 cell) with different concentration of EDB compound

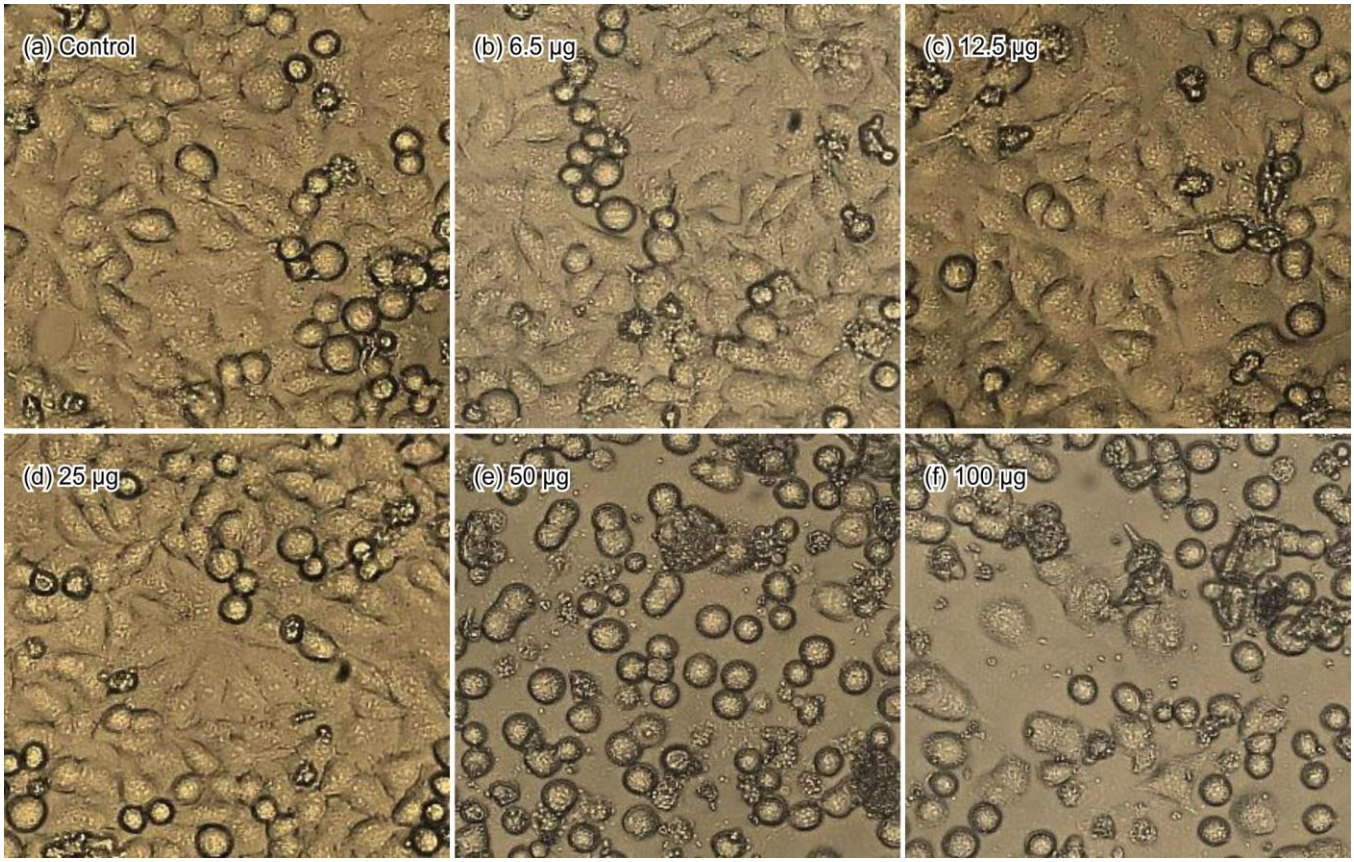


Fig. 17. Anticancer activity of breast cancer (MFCF7 cell) with different concentration of EDB compound

rations and exhibited good agreement between the experimental FT-IR/FT-Raman spectra and the corresponding theoretical frequencies. Mulliken charge analysis revealed significant charge delocalization over the oxygen atoms and selected carbon atoms of the EDB molecule. NBO analysis indicated notable donor–acceptor interactions through Lewis and non-Lewis orbitals, contributing to molecular stabilization. The experimental UV-Vis spectrum exhibited an absorption maximum at 295 nm, which showed good agreement with the TD-DFT results obtained at the B3LYP/6-311G(d,p) level. Thermal analysis demonstrated that EDB remains stable up to approximately 130 ºC, while major decomposition occurs in the temperature range of 200-360 ºC. The HOMO-LUMO energy gap was calculated to be 5.02 eV, indicating good molecular stability and charge delocalization. The calculated chemical softness was 0.19 $eV^{-1}$. MEP analysis identified the oxygen-containing groups (O–H, C=O and C–O) as electron-rich reactive sites. Electron–hole analysis indicated that the second excited state plays the most significant role in the electronic transition process. RDG analysis revealed weak van der Waals interactions, mainly involving O–H···O–H and C=O···H contacts, while ELF and LOL analyses confirmed electron localization around oxygen atoms and low Pauli repulsion in the carbon framework. Drug-likeness and BBB analyses suggested favorable pharmacokinetic properties and potential brain permeability. EDB exhibited antibacterial activity against both Gram-positive and Gram-negative bacteria and inhibited microbial growth at low concentrations. Molecular docking showed binding energies of -4.38 kcal/mol (5TWZ) and -3.32 kcal/mol (5C5S), supporting the observed cytotoxic activity against MCF-7 and A549 cell lines and suggesting the potential of EDB as an anticancer candidate.

## ACKNOWLEDGEMENTS

The authors acknowledge Quantum Computational Research Lab (QCR-Lab) in St. Joseph's College of Arts and Science (Autonomous), Cuddalore, India, for computational purpose. The authors also acknowledge Dr. D. Jayarajan, Head, Department of Microbiology, Divine Mother College, Korkadu, Puducherry, India, for valuable support in antimicrobial and MIC studies and also thank Dr. Rajendran Venkatesh, Asstt. Prof., Cancer Nanobiotechnology Lab, Department of Research, Saveetha College of Nursing, Saveetha Institute of Medical and Technical Sciences, Chennai, India for cancer cell line analysis.

## CONFLICT OF INTEREST

The authors declare that there is no conflict of interests regarding the publication of this article.

## DECLARATION OF AI-ASSISTED TECHNOLOGIES

During the preparation of this manuscript, the authors used an AI-assisted tool(s) to improve the language. The authors reviewed and edited the content and take full responsibility for the published work.

## REFERENCES


1. Z.F. Tao, L.A. Hasvold, J.D. Leverson, E.K. Han, R. Guan, E.F. Johnson, V.S. Stoll, K.D. Stewart, G. Stamper, N. Soni, J.J. Bouska, Y. Luo, T.J. Sowin, N.H. Lin, V.S. Giranda, S.H. Rosenberg and T.D. Penning, *J. Med. Chem.*, **52**, 6621 (2009); https://doi.org/10.1021/jm900943h
2. R.K. Singh, S. Kumar, D.N. Prasad and T.R. Bhardwaj, *Eur. J. Med. Chem.*, **151**, 401 (2018); https://doi.org/10.1016/j.ejmech.2018.04.001
3. A.Y. Spivak, D.A. Nedopekina, R.R. Gubaidullin, E.V. Davletshin, A.A. Tukhbatullin, V.A. D'yakonov, M.M. Yunusbaeva, L.U. Dzhemileva and U.M. Dzhemilev, *Med. Chem. Res.*, **30**, 940 (2021); https://doi.org/10.1007/s00044-021-02702-z
4. V. Kumar, K. Kaur, G.K. Gupta and A.K. Sharma, *Eur. J. Med. Chem.*, **69**, 735 (2013); https://doi.org/10.1016/j.ejmech.2013.08.053
5. C. Bissantz, B. Kuhn, and M. Stahl, *J. Med. Chem.*, **53**, 5061 (2010); https://doi.org/10.1021/jm100112j
6. A. Viji, P. Sivaprakash, R. Vijayakumar, V. Balachandran, C. Bathula, H.S. Kim and I. Kim, *J. Mol. Struct.*, **1321**, 140002 (2025); https://doi.org/10.1016/j.molstruc.2024.140002
7. T. Mosmann, *J. Immunol. Methods*, **65**, 55 (1983); https://doi.org/10.1016/0022-1759(83)90303-4
8. A. Monks, D. Scudiero, P. Skehan, R. Shoemaker, K. Paull, D. Vistica, C. Hose, J. Langley, P. Cronise, A. Vaigro-Wolff, M. Gray-Goodrich, H. Campbell, J. Mayo and M. Boyd, *J. Natl. Cancer Inst.*, **83**, 757 (1991); https://doi.org/10.1093/jnci/83.11.757
9. M.J. Frisch, G.W. Trucks, H.B. Schlegel, G.E. Scuseria, M.A. Robb, J.R.G. Cheeseman, Scalmani, V. Barone, B. Mennucci, G.A. Petersson, H. Nakatsuji, M. Caricato,X. Li, H.P. Hratchian, A.F. Izmaylov, J. Bloino, G. Zheng, J.L. Sonnenberg, M. Hada,M. Ehara, K. Toyota, R. Fukuda, J. Hasegawa, M. Ishida, T. Nakajima, Y.Honda, O. Kitao, H. Nakai, T. Vreven, J.A. Montgomery Jr., J.E. Peralta, F. Ogliaro, M.Bearpark, J.J. Heyd, E. Brothers, K.N. Kudin, V.N. Staroverov, R. Kobayashi, J. Normand, K. Raghavachari, A. Rendell, J.C. Burant, S.S. Iyengar, J. Tomasi, M. Cossi, N. Rega, J. M. Millam, M. Klene, J.E. Knox, J.B. Cross, V. Bakken, C. Adamo, J. Jaramillo, R. Gomperts, R.E. Stratmann, O. Yazyev, A.J. Austin, R. Cammi, C. Pomelli, J.W. Ochterski, R.L. Martin, K. Morokuma, V.G. Zakrzewski, G.A. Voth, P. Salvador, J.J. Dannenberg, S. Dapprich, A.D. Daniels, O. Farkas, J.B. Foresman, J.V. Ortiz, J. Cioslowski, D.J. Fox, Gaussian 09, Revision A.02, Gaussian, Inc., Wallingford CT (2009).
10. R. Dennington, T. Keith and J. Millan, Gauss View, Version 5.08, Semichem. Inc., Shawnee, Mission (2009).
11. M.H. Jamroz, *Spectrochim. Acta A Mol. Biomol. Spectrosc.*, **114**, 220 (2013); https://doi.org/10.1016/j.saa.2013.05.096
12. E.D. Gladening, A.E. Reed, J.E. Carpenter and F. Weinhold, NBO 3.1, Theoretical Chemistry Institute, University of Wisconsin, Madison, WI (1998).
13. E. Cances, B. Mennucci and J. Tomasi, *J. Chem. Phys.*, **107**, 3032 (1997); https://doi.org/10.1063/1.474659
14. B. Mennucci and J. Tomasi, *J. Chem. Phys.*, **106**, 5151 (1997); https://doi.org/10.1063/1.473558
15. N.M. O'boyle, A.L. Tenderholt and K.M. Langner, *J. Comput. Chem.*, **29**, 839 (2008); https://doi.org/10.1002/jcc.20823
16. T. Lu and F. Chen, *J. Comput. Chem.*, **33**, 580 (2012); https://doi.org/10.1002/jcc.22885
17. W. Humphrey, A. Dalke and K. Schultan, *J. Mol. Graph.*, **14**, 33 (1996); https://doi.org/10.1016/0263-7855(96)00018-5
18. A. Lagunin, A. Stepanchikova, D. Filimonov and V. Poroikov, *Bioinformatics*, **16**, 747 (2000); https://doi.org/10.1093/bioinformatics/16.8.747
19. W.L. Delano, The Pymol Molecular Graphics System. Delano Scientific, LLC, Copyright, 2002.
20. G.M. Morris and W. Ruth Huey, *J. Comput. Chem.*, **30**, 2785 (2009); https://doi.org/10.1002/jcc.21256
21. G.M. Morris and S. David, *Hart Richard K. Belew. J. Comput. Chem.*, **19**, 1639 (1998);
22. R. Huey, G.M. Morris, A.J. Olson and D.S. Goodsell, *J. Comput. Chem.*, **28**, 1145 (2007); https://doi.org/10.1002/jcc.20634
23. K. Gopalakrishnan, G. Sowmiya, K. Sekar, S.S. Sheik, *Protein Pept. Lett.*, **14**, 669 (2007); https://doi.org/10.2174/092986607781483912
24. X.-J. Shen, Q.-Z. Zhang, S.X. Wang, Y.J. Zhang and X.-H. Zheng, *Acta Cryst.*, **67**, 03233 (2011); https://doi.org/10.1107/S1600536811044965
25. F.A. Allen, *Acta Crystallogr. B*, **58**, 380 (2002); https://doi.org/10.1107/S0108768102003890
26. İ. Çapan, S. Servi, İ. Yıldırım and Y. Sert, *ChemistrySelect*, **6**, 5838 (2021); https://doi.org/10.1002/slct.202101086
27. M. Amalanathan, V.K. Rastogi, I. Hubert Joe, M.A. Palafox and R. Tomar, *Spectrochim. Acta A Mol. Biomol. Spectrosc.*, **78**, 1437 (2011); https://doi.org/10.1016/j.saa.2011.01.023
28. M. Szafran, A. Komasa and E. Bartoszak-Adamska, *J. Mol. Struct. THEOCHEM*, **827**, 101 (2007); https://doi.org/10.1016/j.molstruc.2006.05.012
29. G. Varsanyi, Vibrational Spectra of Benzene Derivatives, Academic Press: New York (1980).
30. G. Rauhut and P. Puley, *J. Phys. Chem.*, **99**, 3093 (1995); https://doi.org/10.1021/j100010a019
31. H. Singh, S. Singh, A. Srivastava, P. Tandon, P. Bharti, S. Kumar and R. Maurya, *Spectrochim. Acta A Mol. Biomol. Spectrosc.*, **120**, 405 (2014); https://doi.org/10.1016/j.saa.2013.10.045
32. Y. Tao, L. Han, Y. Han and Z. Liu, *Spectrochim. Acta A Mol. Biomol. Spectrosc.*, **137**, 1078 (2015); https://doi.org/10.1016/j.saa.2014.08.151
33. G. Socrates, Infrared Characteristic Group Frequencies, John Wiley & Sons, New York (1980).
34. V. Arjunan, T. Rani, K. Santhanalakshmi and S. Mohan, *Spectrochim. Acta A Mol. Biomol. Spectrosc.*, **79**, 1386 (2011); https://doi.org/10.1016/j.saa.2011.04.073
35. V. Krishnakumar, K. Murugeswari and N. Surumbarkuzhali, *Spectrochim. Acta A Mol. Biomol. Spectrosc.*, **114**, 410 (2013); https://doi.org/10.1016/j.saa.2013.05.047
36. J. Sharmi Kumar, T.S. Renuga devi, G.R. Ramkumar and A. Bright, *Spectrochim. Acta A Mol. Biomol.Spectrosc.*, **152**, 509 (2016); https://doi.org/10.1016/j.saa.2015.07.084
37. R.M. Silverstein, G.C. Bassler, T.C. Morill, Spectrometric Identification of Organic Compounds, Wiley, New York (1974).
38. N. Shanmugapriya, V. Balachandran, B. Revathi, B. Narayanan, V.V. Salion, K. Vanasundari and C. Sivakumar, *Heliyon*, **7**, e07634 (2021); https://doi.org/10.1016/j.heliyon.2021.e07634
39. M. Arivazhagan and J. Senthil Kumar, *Spectrochim. Acta A Mol. Biomol. Spectrosc.*, **137**, 490 (2015); https://doi.org/10.1016/j.saa.2014.08.054
40. K. Fukui, *Science*, **218**, 747 (1982); https://doi.org/10.1126/science.218.4574.747
41. K. Fukui, T. Yonezawa and H. Shingu, *J. Chem. Phys.*, **20**, 722 (1952); https://doi.org/10.1063/1.1700523
42. L. Padmaja, C. Ravikumar, D. Sajan, I. Hubert Joe, V.S. Jayakumar, G.R. Pettit and O. Faurskov Nielsen, *J. Raman Spectrosc.*, **40**, 419 (2009); https://doi.org/10.1002/jrs.2145
43. C. Ravikumar, I.H. Joe and V.S. Jayakumar, *Chem. Phys. Lett.*, **460**, 552 (2008); https://doi.org/10.1016/j.cplett.2008.06.047
44. D.A. Dhas, I.H. Joe, S.D.D. Roy and T.H. Freeda, *Spectrochim. Acta A Mol. Biomol. Spectrosc.*, **77**, 36 (2010); https://doi.org/10.1016/j.saa.2010.04.020
45. P. Winget, J.D. Thompson, J.C. Crame and D.G. Truhiar, *J. Phys. Chem. A*, **106**, 5160 (2002); https://doi.org/10.1021/jp020277g
46. Z. Jia Z. H. Pang H., H. Li X. Wang, *Theor. Chem. Acc.*, **138**, 113 (2019); https://doi.org/10.1007/s00214-019-2502-6
47. E. Eunice, J.C. Prasana, S. Muthu and A. Anuradha, *Polycycl. Aromat. Compd.*, **43**, 5747 (2023); https://doi.org/10.1080/10406638.2022.2107688

48. K. Arulaabaranam, G. Mani and S. Muthu, *Chem. Data. Collect.*, **29**, 1000525 (2020); https://doi.org/10.1016/j.cdc.2020.100525
49. N. Issaoui, H. Ghalla, S.A. Brandan, F. Bardak, H.T. Flakus, A. Atac and B. Oujia, *J. Mol. Struct.*, **1135**, 209 (2017); https://doi.org/10.1016/j.molstruc.2017.01.074
50. C.A. Lipinski, F. Lombardo, B.W. Dominy and P.J. Feeney, *Adv. Drug Deliv. Rev.*, **23**, 3 (1997); https://doi.org/10.1016/S0169-409X(96)00423-1
51. A. Daina, O. Michielin and V. Zoete, *Sci. Rep.*, **7**, 42717 (2017); https://doi.org/10.1038/srep42717
52. R. Kato, W. Zeng, V.B. Siramshetty, J. Williams, M. Kabir, N. Hagen, E.C. Padilha, A.Q. Wang, E.A. Mathé, X. Xu and P. Shah, *Front. Pharmacol.*, **14**, 1291246 (2023); https://doi.org/10.3389/fphar.2023.1291246
53. A. Daina and V. Zoete, *ChemMedChem*, **11**, 1117 (2016); https://doi.org/10.1002/cmdc.201600182
54. H. Pajouhesh and G.R. Lenz, *NeuroRx*, **2**, 541 (2005); https://doi.org/10.1602/neurorx.2.4.541
55. S. Shityakov, W. Neuhaus, T. Dandekar and C. Förster, *Int. J. Comput. Biol. Drug Des.*, **6**, 146 (2013); https://doi.org/10.1504/IJCBDD.2013.052195
56. M. Elmeliegy, M. Vourvahis, C. Guo and D.D. Wang, *Clin. Pharmacokinet.*, **59**, 699 (2020); https://doi.org/10.1007/s40262-020-00867-1
57. N.T. Abdel-Ghani, M.F. Abo El-Ghar and A.M. Mansour, *Spectrochim. Acta*, **104**, 134 (2013); https://doi.org/10.1016/j.saa.2012.11.038
58. B. Kramer, M. Rarey and T. Lengauer, *Proteins*, **37**, 228 (1999); https://doi.org/10.1002/(SICI)1097-0134(19991101)37:2<228::AID-PROT8>3.0.CO; 2-8